Integral Formulations for the EEG Problem

Jan Kybic, Maureen Clerc, Toufic Abboud, Olivier Faugeras, Renaud Keriven, Théodore Papadopoulo

INRIA

INSTITUT NATIONAL DE RECHERCHE EN INFORMATIQUE ET EN AUTOMATIQUE

Integral Formulations for the EEG Problem

Jan Kybic — Maureen Clerc — Toufic Abboud — Olivier Faugeras — Renaud Keriven — Théo Papadopoulo

N° 4735

February 2003

THÈMES 3 et 4

ISSN 0249-6399 ISRN INRIA/RR--4735--FR+ENG

INRIA
SOPHIA ANTIPOLIS

Integral Formulations for the EEG Problem

Jan Kybic, Maureen Clerc, Toufic Abboud*, Olivier Faugeras,
Renaud Keriven, Théo Papadopoulo

Thèmes 3 et 4 — Interaction homme-machine,
images, données, connaissances — Simulation et optimisation
de systèmes complexes
Projet Odyssée†

Rapport de recherche n° 4735 — February 2003 — 37 pages

Abstract: The forward electro-encephalography (EEG) problem involves finding a potential V from the Poisson equation $\nabla \cdot (\sigma \nabla V) = f$, in which f represents electrical sources in the brain, and σ the conductivity of the head tissues. In the piecewise constant conductivity head model, this can be accomplished by the Boundary Element Method (BEM) using a suitable integral formulation. Most previous work is based on the same integral formulation, based on a double-layer potential. In this article we detail several alternative possibilities. We present a dual approach which involves a single-layer potential. Finally, we propose a symmetric formulation, which combines single and double-layer potentials, and which is new to the field of EEG, although it has been applied to other problems in electromagnetism. The three methods have been evaluated numerically using a semi-realistic geometry with known analytical solution, and the symmetric method achieves a significantly higher accuracy.

Key-words: Boundary Element Method, Poisson equation, integral method, EEG

* CMAP, CNRS UMR 7641, Ecole Polytechnique, 91128 Palaiseau
† Odyssée is a joint project between ENPC - ENS Ulm - INRIA.

Unité de recherche INRIA Sophia Antipolis
2004, route des Lucioles, BP 93, 06902 Sophia Antipolis Cedex (France)
Téléphone : +33 4 92 38 77 77 —Télécopie : +33 4 92 38 77 65

Formulations intégrales pour le problème de l'EEG

Résumé : Le problème direct de l'électro-encéphalographie (EEG) consiste à résoudre l'équation de Poisson $\nabla \cdot (\sigma \nabla V) = f$, où f représente les sources électriques dans le cerveau, et σ la conductivité des tissus constituant la tête. Avec un modèle de conductivité constante par morceaux, ce problème peut être résolu par éléments finis surfaciques, à partir d'une formulation intégrale appropriée. Les travaux antérieurs ont systématiquement utilisé la même formulation intégrale, basée sur un potentiel double couche. Dans cet article, nous détaillons d'autres formulations possibles. Nous présentons une formulation duale avec un potentiel simple couche. Puis nous proposons une formulation symétrique, qui combine des potentiels simple et double couche, et qui est nouvelle dans le domaine de l'EEG, bien qu'ayant été appliquée à d'autres problèmes en électromagnétisme. Une comparaison de la précision des trois méthodes exposées a été mise en œuvre, pour une géométrie semi-réaliste, et démontre la supériorité de la méthode symétrique.

Mots-clés : Eléments finis surfaciques, équation de Poisson, méthode intégrale, EEG

1 Introduction

Electroencephalography (EEG) [1] is a non-invasive method of measuring the electrical activity of the brain. To reconstruct the sources in the brain, an accurate forward model of the head must be established. The so called *forward problem* addresses the calculation of the electric potential V on the scalp for a known configuration of the sources, provided that the physical properties of the head tissues (conductivities) are known. Note that the same forward model can be directly used for magnetoencephalography (MEG) [2, 3] as well, since the magnetic field $\mathbf{B}$ can be calculated from the potential V by simple integration [4].

1.1 Problem definition

The quasi-static approximation of Maxwell equations [5] in a conducting environment yields the fundamental Poisson equation

$$\nabla \cdot \left(\sigma \nabla V\right) = f = \nabla \cdot \mathbf{J}^{\mathrm{p}} \quad \text{in } \mathbb{R}^3 \tag{1}$$

where V (in Volts) is the unknown electric potential, $\sigma\,[(\Omega \cdot \mathrm{m})^{-1}]$ is the conductivity, and f is the divergence of the current source density $\mathbf{J}^{\mathrm{p}}\,[\mathrm{A/m^2}]$, all supposed known in the forward problem.

We shall concentrate on a piecewise constant conductivity head model, such as shown in Fig. 1, with connected open sets Ω_i, separated by surfaces S_j. Note that for the sake of notational simplicity, in this article we only consider nested regions with interfaces $S_i = \partial\Omega_i \cap \partial\Omega_{i+1}$. However, extension to other topologies is possible and straightforward.

The outermost volume Ω_{N+1} extends to infinity and in the EEG/MEG problem treated here the corresponding conductivity σ_{N+1} (the conductivity of the air) is considered to be 0. This implies that there can be no source in Ω_{N+1}. The extension to $\sigma_{N+1} \neq 0$ is trivial.

1.2 Notation

We use the notation $\partial_{\mathbf{n}} V = \mathbf{n} \cdot \nabla V$ to denote the partial derivative of V in the direction of a unit vector $\mathbf{n}$, normal to an interface S_j, $j = 1, \ldots, N$. A function f considered on the interface S_j will be denoted f_{S_j}. We define the jump of a function $f : \mathbb{R}^3 \to \mathbb{R}$ at interface S_j as

$$[f]_j = f^-_{S_j} - f^+_{S_j},$$

the functions f^- and f^+ on S_j being respectively the interior and exterior limits of f:

$$\text{for } \mathbf{r} \in S_j, \qquad f^{\pm}_{S_j}(\mathbf{r}) = \lim_{\alpha \to 0^{\pm}} f(\mathbf{r} + \alpha \mathbf{n}).$$

Note that these quantities depend on the orientation of $\mathbf{n}$, which is taken outward by default, as shown in Fig. 1.

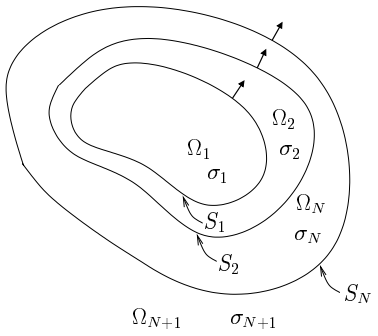

Figure 1: The head is modeled as a set of nested regions $\Omega_1, \ldots, \Omega_{N+1}$ with constant conductivities $\sigma_1, \ldots, \sigma_{N+1}$, separated by interfaces $S_1, \ldots, S_N$. Arrows indicate the normal directions (outward).

1.3 Connected Laplace problems

Thanks to the piecewise constant conductivity, we can factor out σ from (1) to yield a set of Laplace problems connected by boundary conditions:

$$\sigma_i \Delta V = f \quad \text{in } \Omega_i, \text{ for all } i = 1 \ldots N+1 \tag{2}$$

$$\big[V\big]_j = \big[\sigma \partial_{\mathbf{n}} V\big]_j = 0 \quad \text{on } S_j, \text{ for all } j = 1 \ldots N \tag{3}$$

Physically, the boundary condition $[V]_j = 0$ imposes the continuity of the potential across the interfaces. The quasi-static assumption implies the continuity of the current (charge) flow across the interfaces, which is expressed by the second boundary condition $[\sigma \partial_{\mathbf{n}} V]_j = 0$, as $\sigma \partial_{\mathbf{n}} V = \mathbf{n} \cdot \sigma E$ is precisely the density of current. Mathematically, both boundary conditions come from considering (1) on the boundaries.

1.4 Boundary Element Method

The Boundary Element Method (BEM) [6, 7] is today a classical way of solving the forward problem. The advantage of BEM with respect to FDM (finite difference method) or FEM (finite element method) resides in the fact that it only uses as unknowns the values on the interfaces between regions with different conductivities, as oposed to considering values everywhere in the volume. This reduces the dimensionality of the problem and the number of unknowns, and only requires the use of surface triangulation meshes, avoiding the difficult construction of the volume discretization needed for the FEM.

1.5 Inaccuracy of BEM implementations

So far the main disadvantage of using BEM in the EEG/MEG forward problem has been that in all known implementations the precision drops unacceptably when the distance d of the source to one of the surfaces becomes comparable to the size h of the triangles in the mesh. This seriously hinders the usefulness of the BEM, as the sources which are measured by EEG/MEG are often supposed to lie in the cortex, which is only a few millimeters thick. Although the problem is widely acknowledged [8–11], no satisfactory solution has been found so far. Replacing the collocation by the Galerkin method [8, 12] for the resolution of the integral equations improves the precision only partially. The problem has largely been disregarded, or sometimes avoided at the expense of excessively simplifying the model: some authors propose to omit either the outer cortex boundary, or the skull, claiming that these simplifications are inconsequential for the localization accuracy [13, 14]. Unfortunately, our experiments do not support this claim and there is direct and indirect evidence [15, 16] to show that accurate models are essential for accurate reconstruction. Note however, that the MEG reconstruction is reported to be less affected by modeling errors compared to EEG.

1.6 Proposed new integral formulation

As far as we know, all variants of the BEM applied to the EEG/MEG forward problem are based on the same integral formulation, introduced by Geselowitz [17] in 1967. However, this integral formulation is by no means the only one available. We show that the classical formulation corresponds to a double-layer potential approach. We propose a dual formulation using a single-layer potential. Finally, we present a new formulation, combining single and double-layer potentials. This new approach leads to a symmetric system and turns out to be numerically significantly more accurate than the other two formulations.

1.7 Existing work

There is a large body of literature describing BEM implementations using the double-layer potential formulation for forward and inverse EEG/MEG problems [8, 12, 18–22].

The symmetric formulation has existed in the BEM community for some time [7, 23–25], and the single-layer potential formulation has been used for solving elasticity problems [6, 7]. However, to the best of our knowledge, neither the symmetric approach nor the single-layer formulation have so far been applied to the EEG/MEG problem.

1.8 Organization of this article

We start in Section 2 by presenting the mathematical results needed for the Boundary Element Method. Section 3 presents the classical double-layer potential formulation together with its dual formulation in terms of a single-layer potential, and the new symmetric integral formulation, which combines single and double-layer potentials. The discretization and implementation are described in Section 4, followed by experimental results in Section 5.

Technical justifications and remarks relative to Section 2 are relegated to the Appendix and can be skipped at first reading.

2 Representation theorem

The power of the Boundary Element Method is in its conciseness, since it only requires to solve for values defined on surfaces instead of values defined in the volume. The key to this dimension reduction resides in a fundamental representation theorem [6, 7], which we recall in this section.

We define a Green function (see Appendix A)

$$G(\mathbf{r}) = \frac{1}{4\pi\|\mathbf{r}\|} = \frac{1}{4\pi r} \qquad \text{satisfying} \qquad -\Delta G = \delta_0 \ . \tag{4}$$

Given a regular boundary (surface) $\partial\Omega$, we introduce four integral operators $\mathcal{D}, \mathcal{S}, \mathcal{N}, \mathcal{D}^*$, which map a scalar function f on $\partial\Omega$ to another scalar function on $\partial\Omega$:

$$\begin{aligned}
\big(\mathcal{D}f\big)(\mathbf{r}) &= \int_{\partial\Omega} \partial_{\mathbf{n}'} G(\mathbf{r}-\mathbf{r}') f(\mathbf{r}')\,\mathrm{d}s(\mathbf{r}') \ , & \big(\mathcal{S}f\big)(\mathbf{r}) &= \int_{\partial\Omega} G(\mathbf{r}-\mathbf{r}') f(\mathbf{r}')\,\mathrm{d}s(\mathbf{r}') \ , \\
\big(\mathcal{N}f\big)(\mathbf{r}) &= \int_{\partial\Omega} \partial_{\mathbf{n},\mathbf{n}'} G(\mathbf{r}-\mathbf{r}') f(\mathbf{r}')\,\mathrm{d}s(\mathbf{r}') \ , & \big(\mathcal{D}^*f\big)(\mathbf{r}) &= \int_{\partial\Omega} \partial_{\mathbf{n}} G(\mathbf{r}-\mathbf{r}') f(\mathbf{r}')\,\mathrm{d}s(\mathbf{r}') \ .
\end{aligned} \tag{5}$$

where $\mathbf{n}$, resp. $\mathbf{n}'$ are the outward normal vectors at points $\mathbf{r}$, resp. $\mathbf{r}'$. Note that the operator $\mathcal{D}^*$ is the transpose (adjoint) of $\mathcal{D}$ with respect to the $L^2(\partial\Omega)$ scalar product $\langle f, g\rangle = \int_{\partial\Omega} f(\mathbf{r})\, g(\mathbf{r})\,\mathrm{d}s(\mathbf{r}')$. With a slight abuse of notation, we will also consider the values of the above-defined $\big(\mathcal{D}f\big)(\mathbf{r})$ and $\big(\mathcal{S}f\big)(\mathbf{r})$ at any point in $\mathbb{R}^3$, not necessarily at $\mathbf{r} \in \partial\Omega$. The same generalization can be defined also for $\big(\mathcal{N}f\big)(\mathbf{r})$ and $\big(\mathcal{D}^*f\big)(\mathbf{r})$, choosing an arbitrary smooth vector field $\mathbf{n}(\mathbf{r})$.

To simplify the treatment and avoid ambiguity, we choose to work with potential functions vanishing at infinity; more precisely, we say that a function u satisfies a condition $\mathscr{H}$, if simultaneously

$$\begin{cases} \lim\limits_{r\to\infty} r\,|u(\mathbf{r})| < \infty \\ \lim\limits_{r\to\infty} r\frac{\partial u}{\partial r}(\mathbf{r}) = 0 \end{cases} \ ,$$

where $r = \|\mathbf{r}\|$, and $\frac{\partial u}{\partial r}(\mathbf{r})$ denotes the partial derivative of u in the radial direction. The Green function G in (4) satisfies $\mathscr{H}$. The hypothesis about the condition $\mathscr{H}$ corresponds to the physical intuition that a static field far away from all charges is zero. This goes together with the hypothesis we need to make in order to make our initial physical problem uniquely solvable, namely that we are only interested in the field due to sources inside our bounded volumes, i.e. inside the head.

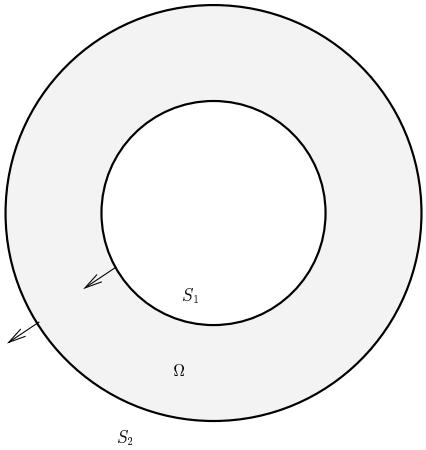

Figure 2: Two-dimensional slice through a volume Ω_2 with a hollow ball topology. Arrows denote the normal orientation.

We are ready now to state the fundamental representation theorem on which the Boundary Element Method is based.

Theorem 1 (Representation Theorem) *Let $\Omega \subseteq \mathbb{R}^3$ be a bounded open set with a regular boundary $\partial\Omega$. Let $u : (\mathbb{R}^3 \backslash \partial\Omega) \to \mathbb{R}$ be a harmonic function ($\Delta u = 0$) in $\mathbb{R}^3 \backslash \partial\Omega$, satisfying the $\mathscr{H}$ condition, and let further $p(\mathbf{r}) \stackrel{def}{=} \partial_{\mathbf{n}} u(\mathbf{r})$. Then*

$$\begin{array}{rrrl} -p = & +\mathcal{N}[u] & -\mathcal{D}^*[p] & \text{for } \mathbf{r} \notin \partial\Omega \\ u = & -\mathcal{D}[u] & +\mathcal{S}[p] & \\ -p^{\pm} = & +\mathcal{N}[u] & +\left(\pm\frac{\mathcal{I}}{2} - \mathcal{D}^*\right)[p] & \text{for } \mathbf{r} \in \partial\Omega \\ u^{\pm} = & \left(\mp\frac{\mathcal{I}}{2} - \mathcal{D}\right)[u] & +\mathcal{S}[p] & \end{array} \tag{6}$$

where $\mathcal{I}$ denotes the identity operator. The equations (6) *also hold for disjoint open sets $\Omega_1, \Omega_2, \Omega_3$ such that $\overline{\Omega}_1 \cup \overline{\Omega}_2 \cup \overline{\Omega}_3 = \mathbb{R}^3$, separated by regular boundaries $\partial\Omega_1 \cap \partial\Omega_2 = S_1$, $\partial\Omega_2 \cap \partial\Omega_3 = S_2$, and $\partial\Omega_1 \cap \partial\Omega_3 = \emptyset$, if we set $\partial\Omega = S_1 \cup S_2$.*

Theorem 1 shows that any harmonic function u in $\mathbb{R}^3 \backslash \partial\Omega$ satisfying $\mathscr{H}$ is determined everywhere by its jump and the jump of its derivative across the boundary $\partial\Omega$, whether $\partial\Omega$ is a single surface, or two surfaces as in the case of a nested topology Fig. 2. This is a very deep result, showing the strong constraints imposed by the harmonicity. It helps us to understand why we can solve a 3D problem by considering only quantities on a 2D surface. For additional notes and a sketch of a proof, we refer the reader to Appendix 2.

2.1 Single and double-layer potentials

From the equations (6) in Theorem 1, we see that the harmonic function u can be represented using two functions $\mu = -[u]$ and $\xi = [p]$ defined on $\partial\Omega$. Historically, the $\mathcal{S}\xi$ part of (6) is called a *single-layer potential*. The single-layer potential is continuous when crossing $\partial\Omega$, while its normal derivative is not; $\left[\mathcal{S}\xi\right]_{\partial\Omega} = 0$, $\left[\partial_{\mathbf{n}}\mathcal{S}\xi\right]_{\partial\Omega} \neq 0$. On the other hand, the second part, $\mathcal{D}\mu$, called a *double-layer potential*, jumps over $\partial\Omega$, while its normal derivative does not; $\left[\mathcal{D}\mu\right]_{\partial\Omega} \neq 0$, $\left[\partial_{\mathbf{n}}\mathcal{D}\mu\right]_{\partial\Omega} = 0$. Refer to Appendix G for more detail on single/double-layer potentials.

To apply the single/double-layer potentials to our nested-region model in Fig. 1, we simply add up the contributions from all interfaces, $u_s = \sum_i \mathcal{S}\xi_{S_i}$ resp. $u_d = \sum_i \mathcal{D}\mu_{S_i}$. This yields single, resp. double-layer, potentials with the same jump properties as in the single interface case (see Appendix H). Further on, we shall need in particular the following two relations, easily obtainable from (6) by additivity:

$$\partial_{\mathbf{n}} u_s^{\pm}(\mathbf{r}) = \mp\frac{\xi_{S_j}}{2} + \sum_{i=1}^{N} \mathcal{D}^*_{ji}\xi_{S_i} \quad \text{for } \mathbf{r} \in S_j \tag{7}$$

$$u_d^{\pm}(\mathbf{r}) = \pm\frac{\mu_{S_j}}{2} + \sum_{i=1}^{N} \mathcal{D}_{ji}\mu_{S_i} \quad \text{for } \mathbf{r} \in S_j\ . \tag{8}$$

The operators $\mathcal{D}^*_{ji}$ and $\mathcal{D}_{ji}$ are restrictions of $\mathcal{D}^*$ and $\mathcal{D}$: they act on a function defined on S_i and yield a function defined on S_j. This convention is used consistently in the remainder of this paper.

3 Integral formulations

Let us use Theorem 1 to obtain integral formulations for the original multiple interface problem (3). We now need to cope with the presence of sources which make the solution non-harmonic. We shall start from a homogeneous solution v that takes the source terms into account, but does not necessarily respect all boundary conditions. Then we add to v a harmonic function u to obtain a complete solution V which simultaneously respects the Laplace equation $\sigma\Delta V = f$ and the boundary conditions (3). Three different ways of achieving this are described in this section. We shall always assume V to satisfy condition $\mathscr{H}$, which amounts to imposing a zero potential infinitely far from all sources.

3.1 Dipole source

The source most commonly used to represent electrical activity in the brain is a "current dipole"[1] [3]. It represents an infinitely small oriented source of current positioned at $\mathbf{r}_0$, with dipolar moment $\mathbf{q}$, and is defined by $\mathbf{J}_{\text{dip}}(\mathbf{r}) = \mathbf{q}\,\delta_{\mathbf{r}_0}(\mathbf{r})$. The corresponding source term in

[1] This is a traditional name, used because the quantity $\mathbf{q}$ has the units of $[\text{A}\cdot\text{m}]$.

the Laplace equation is $f_{\text{dip}} = \nabla \cdot \mathbf{J}_{\text{dip}} = \mathbf{q} \cdot \nabla \delta_{\mathbf{r}_0}$, which yields the homogeneous domain potential

$$v_{\text{dip}}(\mathbf{r}) = \frac{1}{4\pi} \frac{\mathbf{q} \cdot (\mathbf{r}_0 - \mathbf{r})}{\|\mathbf{r}_0 - \mathbf{r}\|^3} \ . \tag{9}$$

3.2 Homogeneous solution

We decompose the sources f from (1) into domains as $f = \sum_{i=1}^{N} f_{\Omega_i}$ such that $f_{\Omega_i} = f \cdot 1_{\Omega_i}$, where 1_{Ω_i} is the indicator function of Ω_i (hence $f_{\Omega_i} = 0$ outside Ω_i). Recall that no source lies in Ω_{N+1}; we also assume that no source lies on any boundary S_i.

For each partial source term f_{Ω_i} we calculate the homogeneous medium solution $v_{\Omega_i}(\mathbf{r}) = -f_{\Omega_i} * G(\mathbf{r})$. The convolution theorem shows that $\Delta v_{\Omega_i} = -f_{\Omega_i} * \Delta G(\mathbf{r})$ and $\Delta v_{\Omega_i} = f_{\Omega_i}$ follows from the properties of the Green function (4). Thanks to the choice of G in (4), the functions v_{Ω_i} satisfy the $\mathscr{H}$ condition, provided that the f_{Ω_i} are compactly supported. This is true by construction for $\Omega_1, \ldots, \Omega_N$ since each of these domains is bounded.

3.3 Multiple domains

There are various ways of combining the individual homogeneous solutions v_{Ω_i} from domains Ω_i into a global homogeneous v. First we consider a function v_s constructed as:

$$v_s = \sum_{i=1}^{N} v_{\Omega_i} / \sigma_i \ . \tag{10}$$

We easily verify that it solves the Laplace equation $\sigma \Delta v_s = f$:

$$\sigma \Delta v_s = \sigma \sum_{i=1}^{N} \Delta v_{\Omega_i} / \sigma_i = \sigma \sum_{i=1}^{N} \frac{f_{\Omega_i}}{\sigma_i} = \sum_{i=1}^{N} f_{\Omega_i} = f \quad \text{in each } \Omega_i.$$

The function v_s and its derivative $\partial_{\mathbf{n}} v_s$ are continuous across each S_j. In other words, v_s satisfies the boundary conditions $\left[v_s\right]_j = 0$ and $\left[\partial_{\mathbf{n}} v_s\right]_j = 0$ for all j, but not the boundary condition $\left[\sigma \partial_{\mathbf{n}} v_s\right]_j = 0$. The function v_s will be used in the single-layer approach, Section 3.4, whence the subscript s.

In a dual fashion, we would like to consider the function $\tilde{v}_d(\mathbf{r}) = \sigma^{-1}(\mathbf{r}) \sum_{i=1}^{N} v_{\Omega_i}$ that satisfies $\sigma \Delta \tilde{v}_d = f$ and the boundary condition $\left[\sigma \partial_{\mathbf{n}} \tilde{v}_d\right]_j = 0$. Unfortunately, $\tilde{v}_d$ is not properly defined in Ω_{N+1} where $\sigma = 0$. Instead, we introduce a function

$$v_d = \sum_{i=1}^{N} v_{\Omega_i} \tag{11}$$

that satisfies the Laplace equation $\Delta v_d = f$ and the boundary conditions $\left[v_d\right]_j = 0$ and $\left[\partial_{\mathbf{n}} v_d\right]_j = 0$ on each surface S_j. This function will be used in the double-layer approach, Section 3.5.

3.4 Single-layer approach

A natural approach to solving (1) consists of representing the potential V in a way which automatically satisfies $[V]_j = 0$ and then adjusting the harmonic part so that the remaining boundary conditions, $[\sigma\partial_{\mathbf{n}}V]_j = 0$, are satisfied as well. We consider $u_s = V - v_s$, with v_s defined by (10). By construction, u_s is harmonic in $\Omega = \Omega_1 \cup \ldots \cup \Omega_N$, since in each Ω_i we have $\sigma_i \Delta u_s = \sigma_i \Delta V - \sigma_i \Delta v_s = f_{\Omega_i} - f_{\Omega_i} = 0$. It is also harmonic in Ω_{N+1}, as both V and v_s are harmonic there. Since $[V]_j = 0$ and $[v_s]_j = 0$ (Section 3.3), we conclude that $[u_s]_j = 0$ across all surfaces S_j. This means that u_s is a single-layer potential for $\Omega = \Omega_1 \cup \ldots \cup \Omega_N$ with the corresponding boundary $\partial\Omega = S_1 \cup \ldots \cup S_N$ (cf Section 2.1).

We use equation (7) for the normal derivative of a single-layer potential. We then use the second set of boundary conditions, $[\sigma\partial_{\mathbf{n}}V] = 0$, implying that $[\sigma\partial_{\mathbf{n}}u_s] = -[\sigma\partial_{\mathbf{n}}v_s]$. We express $[\sigma\partial_{\mathbf{n}}u_s]$ as a function of known quantities:

$$\left[\sigma\partial_{\mathbf{n}}u_s\right]_j = -\left[\sigma\partial_{\mathbf{n}}v_s\right]_j = -(\sigma_j - \sigma_{j+1})\partial_{\mathbf{n}}v_s \quad \text{on } S_j \tag{12}$$

since $\partial_{\mathbf{n}}v_s$ does not "jump" (Section 3.3). Equation (7) yields

$$\left[\sigma\partial_{\mathbf{n}}u_s\right]_j = \sigma_j\partial_{\mathbf{n}}u_s^- - \sigma_{j+1}\partial_{\mathbf{n}}u_s^+ = \frac{\sigma_j + \sigma_{j+1}}{2}\xi_{S_j} + (\sigma_j - \sigma_{j+1})\sum_{i=1}^{N-1}\mathcal{D}_{ji}^*\xi_{S_i}$$

on all $S_1, \ldots, S_N$. Combining this result with (12) we obtain

$$\partial_{\mathbf{n}}v_s = \frac{\sigma_j + \sigma_{j+1}}{2(\sigma_{j+1} - \sigma_j)}\xi_{S_j} - \sum_{i=1}^{N-1}\mathcal{D}_{ji}^*\xi_{S_i} \quad \text{on all } S_j\ . \tag{13}$$

This is a system of N integral equations in the unknown functions ξ_{S_j}. Its solution is unique up to a constant [7] (see also Section J). Once it is solved, the potential u_s for $\mathbf{r} \in S_j$ is determined from

$$u_s(\mathbf{r}) = \sum_{i=1}^{N}\mathcal{S}_{ji}\xi_{S_i}\ ,$$

and the values of V follow from $V = v_s + u_s$.

We observe that V is expressed as an exactly calculable homogeneous medium potential v_s plus a correction term u_s. If the medium is close to homogeneous, the correction is small, which helps to improve the accuracy of this method. This method is to be favored if we are interested in calculating the flow or the current. However, to obtain the potential V, an additional computation is necessary.

3.5 Double-layer approach

The double-layer approach is dual to the single-layer approach. We use a representation satisfying $[\sigma\partial_{\mathbf{n}}V]_j = 0$ by construction and then find conditions on the harmonic part to

satisfy $[V]_j = 0$ as well. Consider a function $u_d = \sigma V - v_d$, with v_d given by (11). By construction, u_d is harmonic in $\Omega = \Omega_1 \cup \ldots \cup \Omega_{N-1}$, because in each Ω_i we have $\Delta u_d = \sigma_i \Delta V - \Delta v_d = f_{\Omega_i} - f_{\Omega_i} = 0$. It is also harmonic in Ω_N, as both V and v_d are harmonic there. Since $[\sigma \partial_{\mathbf{n}} V]_j = 0$ and $[\partial_{\mathbf{n}} v_d]_j = 0$ (Section 3.3), we conclude that $[\partial_{\mathbf{n}} u_d]_j = 0$ on all surfaces S_i. This means that u_d is a double-layer potential for $\Omega = \Omega_1 \cup \ldots \cup \Omega_N$ with the corresponding boundary $\partial\Omega = S_1 \cup \ldots \cup S_N$. We use (8) to express the values of the the double-layer representation. We then use the second set of boundary conditions, $[V]_j = 0$, implying that $\sigma_{j+1}(u_d + v_d)^- = \sigma_j (u_d + v_d)^+$ for all S_j. (This is equivalent to $\sigma_j^{-1}(u_d + v_d)^- = \sigma_{j+1}^{-1}(u_d + v_d)^+$ for $\sigma \neq 0$ and a natural extension thereof for $\sigma = 0$.) We can also express $\mu_{S_i} = -[V] = (\sigma_{i+1} - \sigma_i) V_{S_i}$, where V_{S_i} is the restriction of V to S_i. This yields

$$v_d = \frac{\sigma_j + \sigma_{j+1}}{2} V_{S_j} - \sum_{i=1}^{N} (\sigma_{i+1} - \sigma_i) \mathcal{D}_{ji} V_{S_i} \quad \text{on each } S_j. \tag{14}$$

The function v_d (11) is the solution of $\Delta v_d = f$, corresponding to a homogeneous medium with conductivity equal to one. Recalling that $\mathcal{D}_{ji} V_{S_i}(\mathbf{r}) = \int_{S_i} \frac{\partial}{\partial \mathbf{n}'} G(\mathbf{r} - \mathbf{r}')\, V(\mathbf{r}')\, ds(\mathbf{r}')$ for $\mathbf{r} \in S_j$, we recognize in (14) the classical integral formulation used for EEG and MEG [2, 3, 17, 19, 20]. The advantage of this approach is that it solves directly for V and no additional post-processing step is therefore necessary. As in the single-layer approach, the solution of the system (14) is unique up to a constant [7].

3.6 Symmetric approach

The third, symmetric approach, uses both the single and double-layer potentials. It is based on the theory of Nédélec [7] and is also closely related to algorithms in [23, 24]. However, as far as we know, it has so far never been described for the EEG/MEG problem. In this approach, we consider in each $\Omega_1, \ldots, \Omega_N$ the function

$$u_{\Omega_i} = \begin{cases} V - v_{\Omega_i}/\sigma_i & \text{in } \Omega_i \\ -v_{\Omega_i}/\sigma_i & \text{in } \mathbb{R}^3 \backslash \overline{\Omega}_i \end{cases}.$$

Each u_{Ω_i} is harmonic in $\mathbb{R}^3 \backslash \partial\Omega_i$. The boundary of Ω_i is in our case $\partial\Omega_i = S_{i-1} \cup S_i$. With the orientations of normals indicated in Fig. 3, the jumps of u_i satisfy the relations

$$[u_{\Omega_i}]_i = V_{S_i}, \qquad [u_{\Omega_i}]_{i-1} = -V_{S_{i-1}}\ , \tag{15a}$$

and the jumps of their derivatives

$$[\partial_{\mathbf{n}} u_{\Omega_i}]_i = (\partial_{\mathbf{n}} V)^-_{S_i}, \qquad [\partial_{\mathbf{n}} u_{\Omega_i}]_{i-1} = -(\partial_{\mathbf{n}} V)^+_{S_{i-1}}\ . \tag{15b}$$

We define $p_{S_i} = \sigma_i [\partial_{\mathbf{n}} u_{\Omega_i}]_i = \sigma_i (\partial_{\mathbf{n}} V)^-_{S_i}$. Note that since $[\sigma \partial_{\mathbf{n}} V] = 0$ from (3), we have $p_{S_i} = \sigma_i (\partial_{\mathbf{n}} V)^-_{S_i} = \sigma_{i+1} (\partial_{\mathbf{n}} V)^+_{S_i}$ at the interface S_i. As u_{Ω_i} is harmonic in $\mathbb{R}^3 \backslash \partial\Omega_i$ and

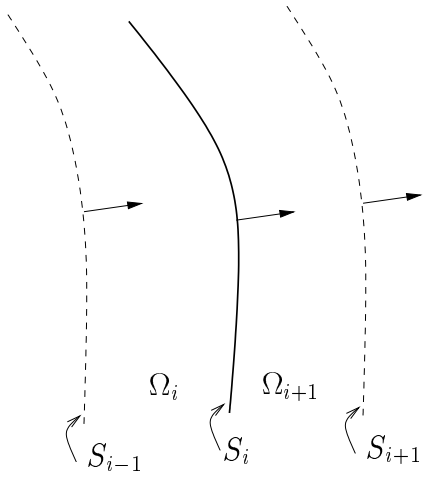

Figure 3: A detail of the nested volume model. Normal vectors are oriented globally outward, as shown. However, when considering for example the surface S_i as the boundary of Ω_{i+1}, the orientation needs to be reversed.

satisfies the condition $\mathscr{H}$, we can apply Theorem 1 to obtain the internal limit on S_i:

$$\left(u_{\Omega_i}\right)^-_{S_i} = \frac{\left[u_{\Omega_i}\right]_{\partial\Omega_i}}{2} - \mathcal{D}_{\partial\Omega_i}\left[u_{\Omega_i}\right]_{\partial\Omega_i} + \mathcal{S}_{\partial\Omega_i}\left[\partial_{\mathbf{n}} u_{\Omega_i}\right]_{\partial\Omega_i}$$

If we break down the jump terms across $\partial\Omega_i = S_{i-1} \cup S_i$ into two parts, corresponding to S_{i-1} and S_i, and if we take into account identities (15a), we obtain

$$\left(u_{\Omega_i}\right)^-_{S_i} = \left(V - v_{\Omega_i}/\sigma_i\right)^-_{S_i} = \frac{V_{S_i}}{2} + \mathcal{D}_{i,i-1}V_{S_{i-1}} - \mathcal{D}_{ii}V_{S_i} - \sigma_i^{-1}\mathcal{S}_{i,i-1}p_{S_{i-1}} + \sigma_i^{-1}\mathcal{S}_{ii}p_{S_i} \quad (16)$$

A similar analysis applies to $u_{\Omega_{i+1}}$. Theorem 1 gives as an external limit on S_i with respect to Ω_{i+1}:

$$\left(u_{\Omega_{i+1}}\right)^+_{S_i} = -\frac{\left[u_{\Omega_{i+1}}\right]_{\partial\Omega_{i+1}}}{2} - \mathcal{D}_{\partial\Omega_{i+1}}\left[u_{\Omega_{i+1}}\right]_{\partial\Omega_{i+1}} + \mathcal{S}_{\partial\Omega_{i+1}}\left[\partial_{\mathbf{n}} u_{\Omega_{i+1}}\right]_{\partial\Omega_{i+1}}$$

We substitute for the values of $[u_{\Omega_{i+1}}]$ and $[\partial_{\mathbf{n}} u_{\Omega_{i+1}}]$ from (15a) and break down the terms on $\partial\Omega_{i+1} = S_i \cup S_{i+1}$, to obtain

$$\left(u_{\Omega_{i+1}}\right)^+_{S_i} = \left(V - v_{\Omega_{i+1}}/\sigma_{i+1}\right)^+_{S_i} = \frac{V_{S_i}}{2} + \mathcal{D}_{ii}V_{S_i} - \mathcal{D}_{i,i+1}V_{S_{i+1}} - \sigma_{i+1}^{-1}\mathcal{S}_{ii}p_{S_i} + \sigma_{i+1}^{-1}\mathcal{S}_{i,i+1}p_{S_{i+1}} \quad (17)$$

We subtract (16) and (17); given that the functions V, $v_{\Omega_{i+1}}$, v_{Ω_i} are continuous across S_i and their internal and external limits hence coincide:

$$\sigma_{i+1}^{-1}(v_{\Omega_{i+1}})_{S_i} - \sigma_i^{-1}(v_{\Omega_i})_{S_i} = \mathcal{D}_{i,i-1}V_{S_{i-1}} - 2\mathcal{D}_{ii}V_{S_i} + \mathcal{D}_{i,i+1}V_{S_{i+1}} - \sigma_i^{-1}\mathcal{S}_{i,i-1}p_{S_{i-1}} + (\sigma_i^{-1} + \sigma_{i+1}^{-1})\mathcal{S}_{ii}p_{S_i} - \sigma_{i+1}^{-1}\mathcal{S}_{i,i+1}p_{S_{i+1}} \quad \text{for } i = 1, \ldots, N \quad (18)$$

Using the same approach, we evaluate the quantities $\left(\sigma_i \partial_{\mathbf{n}} u_{\Omega_i}\right)_{S_i}^{-} = \left(p - \partial_{\mathbf{n}} v_{\Omega_i}\right)_{S_i}^{-}$ and $\left(\sigma_{i+1}\partial_{\mathbf{n}} u_{\Omega_{i+1}}\right)_{S_i}^{+} = \left(p - \partial_{\mathbf{n}} v_{\Omega_{i+1}}\right)_{S_i}^{+}$ using Theorem 1, subtract the resulting expressions and obtain

$$(\partial_{\mathbf{n}} v_{\Omega_{i+1}})_{S_i} - (\partial_{\mathbf{n}} v_{\Omega_i})_{S_i} = \sigma_i \mathcal{N}_{i,i-1}V_{S_{i-1}} - (\sigma_i + \sigma_{i+1})\mathcal{N}_{ii}V_{S_i} + \sigma_{i+1}\mathcal{N}_{i,i+1}V_{S_{i+1}} - \mathcal{D}_{i,i-1}^{*}p_{S_{i-1}} + 2\mathcal{D}_{ii}^{*}p_{S_i} - \mathcal{D}_{i,i+1}^{*}p_{S_{i+1}} \quad \text{for } i = 1, \ldots, N \quad (19)$$

Here (and in (18)) the terms corresponding to non-existing indices $(0,\ N+1)$ are to be set to zero, as there are no corresponding surfaces. Terms involving p_N must also be set to zero, since $\sigma_{N+1} = 0$ implies $p_N = 0$.

Observe that, unlike in the previous approaches, each surface only interacts with its neighbors. Equations (18) and (19) thus lead to s a block-diagonal symmetric operator matrix, which is displayed in Fig. 4. Note that the vanishing conductivity $\sigma_{N+1} = 0$ is taken into account by effectively chopping off the last line and column of the matrix.

4 Discretization and implementation

The discretization of all the exposed integral methods can be divided into three steps: discretization of the boundaries, discretization of the unknowns, and choice of the test functions, corresponding to the choice of the error measure to discretize the equations.

4.1 Discretization of the boundaries

The first step is to approximate the boundaries by surface meshes. Triangulation is used in the vast majority of cases. Higher-order elements [22] are rarely used for the EEG/MEG problem, despite their potential to improve the modeling accuracy, because of the lack of algorithms to generate meshes with high-order elements from the available data (mostly volumes of anatomical MRI [26, 27]). As a triangulated surface is not regular, some caution is needed in the application of the continuous equations derived above, (cf Appendix K).

4.2 Discretization of the unknowns

The second step consists of approximating the continuous unknowns V, p or ξ using a finite number of basis functions φ_i, for example $V = \sum_i v_i \varphi_i$. The classical choice is the space P0, where a basis function ψ_i equal 1 on triangle T_i and 0 elsewhere. The second possibility is

$$
\begin{bmatrix}
(\sigma_1+\sigma_2)\mathcal{N}_{11} & -2\mathcal{D}^*_{11} & -\sigma_2\mathcal{N}_{12} & \mathcal{D}^*_{12} & & & & & \\
-2\mathcal{D}_{11} & (\sigma_1^{-1}+\sigma_2^{-1})\mathcal{S}_{11} & \mathcal{D}_{12} & -\sigma_2^{-1}\mathcal{S}_{12} & & & & & \\
-\sigma_2\mathcal{N}_{21} & \mathcal{D}^*_{21} & (\sigma_2+\sigma_3)\mathcal{N}_{22} & -2\mathcal{D}^*_{22} & -\sigma_3\mathcal{N}_{23} & \mathcal{D}^*_{23} & & & \\
\mathcal{D}_{21} & -\sigma_2^{-1}\mathcal{S}_{21} & -2\mathcal{D}_{22} & (\sigma_2^{-1}+\sigma_3^{-1})\mathcal{S}_{22} & \mathcal{D}_{23} & -\sigma_3^{-1}\mathcal{S}_{23} & & & \\
 & & -\sigma_3\mathcal{N}_{32} & \mathcal{D}^*_{32} & (\sigma_3+\sigma_4)\mathcal{N}_{33} & -2\mathcal{D}^*_{33} & \dots & & \\
 & & \mathcal{D}_{32} & -\sigma_3^{-1}\mathcal{S}_{32} & -2\mathcal{D}_{33} & (\sigma_3^{-1}+\sigma_4^{-1})\mathcal{S}_{33} & \dots & & \\
 & & & & \vdots & \vdots & \ddots & & \\
 & & & & & & (\sigma_{N-1}+\sigma_N)\mathcal{N}_{N-1,N-1} & -2\mathcal{D}^*_{N-1,N-1} & -\sigma_N\mathcal{N}_{N-1,N} \\
 & & & & & & -2\mathcal{D}_{N-1,N-1} & (\sigma_{N-1}^{-1}+\sigma_N^{-1})\mathcal{S}_{N-1,N-1} & \mathcal{D}_{N-1,N} \\
 & & & & & & -\sigma_N\mathcal{N}_{N,N-1} & \mathcal{D}^*_{N,N-1} & \sigma_N\mathcal{N}_{N,N}
\end{bmatrix}
\begin{bmatrix} V_{S_1} \\ p_{S_1} \\ V_{S_2} \\ p_{S_2} \\ V_{S_3} \\ p_{S_3} \\ \vdots \\ V_{S_N} \end{bmatrix}
=
\begin{bmatrix}
(\partial_{\mathbf{n}} v_{\Omega_1})_{S_1} - (\partial_{\mathbf{n}} v_{\Omega_2})_{S_1} \\
\sigma_2^{-1}(v_{\Omega_2})_{S_1} - \sigma_1^{-1}(v_{\Omega_1})_{S_1} \\
(\partial_{\mathbf{n}} v_{\Omega_2})_{S_2} - (\partial_{\mathbf{n}} v_{\Omega_3})_{S_2} \\
\sigma_3^{-1}(v_{\Omega_3})_{S_2} - \sigma_2^{-1}(v_{\Omega_2})_{S_2} \\
(\partial_{\mathbf{n}} v_{\Omega_3})_{S_3} - (\partial_{\mathbf{n}} v_{\Omega_4})_{S_3} \\
\sigma_4^{-1}(v_{\Omega_4})_{S_3} - \sigma_3^{-1}(v_{\Omega_3})_{S_3} \\
\vdots \\
(\partial_{\mathbf{n}} v_{\Omega_N})_{S_N}
\end{bmatrix}
\tag{20}
$$

Figure 4: System representing the continuous operator version of the symmetric method. Observe that the system is symmetric and block-diagonal. Special care is taken in writing the last block because of the conductivity $\sigma_{N+1} = 0$.

the space P1, with basis functions ϕ_i equal 1 on vertex i, 0 on all other vertices, and linear on each triangle. Let us denote by N_v the number of P1 basis functions and by N_t the number of P0 basis functions, where N_v (resp. N_t) is the number of vertices (resp. triangles) in the mesh. For closed meshes, $N_t = 2(N_v - 2)$. Higher-order basis functions are not useful with triangular meshes, the additional precision being wasted since the total error of the method becomes dominated by the geometrical error.

4.3 Test functions

Third, to convert the continuous equations of discrete variables into a set of discrete equations, we integrate each of them against a set of test functions $\tilde{\varphi}_j$. For example, if the continuous equation is $\mathcal{A}V = V_0$, then the discrete equations will be $\langle \mathcal{A}V, \tilde{\varphi}_i \rangle = \langle V_0, \tilde{\varphi}_i \rangle$. The simplest choice of test functions is a Dirac mass, $\tilde{\varphi}_i = \delta_{\mathbf{x}_i}$. For our model equation, this leads to $\big(\mathcal{A}V\big)(\mathbf{x}_i) = V_0(\mathbf{x}_i)$, imposing the equality at a set of points. This method, called "collocation", is comparatively simple and fast, but often not very accurate. One normally chooses as many collocation points $\mathbf{x}_i$ as there are unknowns v_i. Special care is needed to evaluate the functions at non-regular points of the surface, such as vertices, (see also Appendix K).

4.4 Galerkin methods

Galerkin-type methods replace the pointwise equality by an equality in the mean sense. The test functions $\{\tilde{\varphi}_i\}$ are often chosen equal to the basis functions $\{\varphi_i\}$; this leads to square system matrices. There is an extra integration involved which most of the time needs to be performed numerically. Many times the integrand is singular which augments the difficulty. Galerkin methods are hence more difficult to implement and slower than collocation, but usually more accurate. We shall therefore concentrate on Galerkin methods in the detailed treatment of the three integral formulations that follows.

4.5 Single-layer formulation

The continuous equation (13) obtained in the single-layer approach (3.4) is discretized using a Galerkin method, described above. The single-layer density ξ_{S_k} on S_k is represented as $\xi_{S_k}(\mathbf{r}) = \sum_i x_i^{(k)} \varphi_i^{(k)}(\mathbf{r})$, where φ_i can be either a P0 or P1 function. Taking the scalar product of equation (13) (in which ξ_{S_k} has been discretized) with the same functions $\varphi_i^{(k)}$ yields the following set of equations:

$$\big\langle \partial_{\mathbf{n}} v_s, \varphi_i^{(k)} \big\rangle = \frac{\sigma_k + \sigma_{k+1}}{2(\sigma_{k+1} - \sigma_k)} \Big(\sum_j x_j^{(k)} \big\langle \varphi_i^{(k)}, \varphi_j^{(k)} \big\rangle \Big) - \sum_{l=1}^{N} \sum_j x_j^{(l)} \big\langle \mathcal{D}_{lk}^* \varphi_j^{(l)}, \varphi_i^{(k)} \big\rangle \ . \qquad (21)$$

The explicit matrix form is

$$\underbrace{\begin{bmatrix} \mathsf{J}_1+\mathsf{D}^*_{11} & \mathsf{D}^*_{12} & \mathsf{D}^*_{13} & \dots & \mathsf{D}^*_{1,N} \\ \mathsf{D}^*_{21} & \mathsf{J}_2+\mathsf{D}^*_{22} & \mathsf{D}^*_{23} & \dots & \mathsf{D}^*_{2,N} \\ \mathsf{D}^*_{31} & \mathsf{D}^*_{32} & \mathsf{J}_3+\mathsf{D}^*_{33} & \dots & \mathsf{D}^*_{3,N} \\ \vdots & \vdots & \vdots & \ddots & \vdots \\ \mathsf{D}^*_{N,1} & \mathsf{D}^*_{N,2} & \mathsf{D}^*_{N,3} & \dots & \mathsf{J}_N+\mathsf{D}^*_{N,N} \end{bmatrix}}_{\mathsf{A}} \begin{bmatrix} \mathbf{x}_1 \\ \mathbf{x}_2 \\ \mathbf{x}_3 \\ \vdots \\ \mathbf{x}_N \end{bmatrix} = \begin{bmatrix} \mathbf{b}_1 \\ \mathbf{b}_2 \\ \mathbf{b}_3 \\ \vdots \\ \mathbf{b}_N \end{bmatrix} \tag{22}$$

where the matrices J (which are almost diagonal) are given by

$$\big(\mathsf{J}_k\big)_{ij} = \frac{\sigma_k+\sigma_{k+1}}{2(\sigma_{k+1}-\sigma_k)} \big\langle \varphi_i^{(k)}, \varphi_j^{(k)} \big\rangle,$$

the elements of D^* by

$$\big(\mathsf{D}^*_{kl}\big)_{ij} = -\big\langle \mathcal{D}^*_{kl}\varphi_j^{(l)}, \varphi_i^{(k)} \big\rangle,$$

and the vectors $\mathbf{b}$ and $\mathbf{x}$ by

$$\big(\mathbf{b}_k\big)_i = \big\langle \partial_{\mathbf{n}} v_s, \varphi_i^{(k)} \big\rangle, \qquad \big(\mathbf{x}_k\big)_i = x_i^{(k)} \ .$$

Care is needed in calculating the elements $\big(\mathsf{D}^*_{kk}\big)_{ii}$ because of the singularity of the operator $\mathcal{D}^*$ (see (5)). Some authors adjust the diagonal values to compensate the numerical errors of the rest of the elements using the fact that the sum of the columns of D^*_{kk} is known (see [10] for the double-layer approach). This arises from the fact that the total solid angle $\omega = 4\pi\big(\mathcal{D}_i 1\big)(\mathbf{r})$ must be equal to 4π for all interior points, and from the physical necessity of obtaining a singular matrix (see Appendix J). However, we prefer to set $\big(\mathsf{D}^*_{kk}\big)_{ii} = 0$, which is exact at regular points of flat surfaces (triangles), trivial to compute, and unlike the former approach does not obscure potential accuracy problems. We did not observe a significant difference in accuracy between the two choices.

The system matrix A is full and non-symmetric. The elements of the matrices D^* involve double surface integrals over triangles of the meshes. The inner integrals can be calculated analytically for both P0 and P1 basis functions [19, 28, 29], the outer integral must be calculated numerically, which is most efficiently done using a Gaussian quadrature adapted to triangles [6, 30].

Once $\mathbf{x}$ is known, the potential V is calculated directly as

$$V(\mathbf{r}) = v_d(\mathbf{r}) + \sum_{l=1}^{N-1} \sum_j x_j^{(l)} \left(\mathcal{S}_{lk} \varphi_j^{(l)} \right)(\mathbf{r}) \qquad \text{for} \quad \mathbf{r} \in S_k \ . \tag{23}$$

Note that no approximation is involved here; if $\mathbf{x}$ is known exactly, V can be calculated exactly too.

4.6 Deflation

An important point to note is that the matrix A as presented in (22) is singular (see Appendix J). We "deflate" it [31] using the condition $\langle \xi, 1 \rangle = 0$ (see Section J). For the commonly used basis functions satisfying the partition of unity property[2], this is equivalent to $\sum_i x_i^{(k)} = 0$ on each S_k, and thus $\sum_{ik} x_i^{(k)} = 0$. To impose this, we replace A with $\mathsf{A}' = \mathsf{A} + \omega \mathbf{1}^T \mathbf{1}$, where ω is chosen such that A' is well conditioned. The optimal choice ω is too costly to calculate but the value is not very critical and can be approximated [12, 32]. We use the fact that A is approximately diagonally dominant and we assume that the very first element is representative, which leads to $\omega = \big(\mathsf{A}\big)_{11}/M$, where M is the total number of unknowns. This was found to perform acceptably well. The deflated matrix A' is regular and square and can be inverted by the usual methods.

4.7 Double-layer formulation

The double-layer formulation (14) is discretized using the same approach as the single-layer one, with V_{S_k} on S_k represented as $V_{S_k}(\mathbf{r}) = \sum_i x_i^{(k)} \varphi_i^{(k)}(\mathbf{r})$, where φ_i is either P0 or P1. Taking the scalar product of (14) with $\varphi_i^{(k)}$ yields

$$\Big\langle \sum_{l=1}^{N} v_{\Omega_l}, \varphi_i^{(k)} \Big\rangle = \frac{\sigma_k + \sigma_{k+1}}{2} \Big(\sum_j x_j^{(k)} \big\langle \varphi_i^{(k)}, \varphi_j^{(k)} \big\rangle \Big) - \sum_{l=1}^{N} (\sigma_{l+1} - \sigma_l) \sum_j x_j^{(l)} \big\langle \mathcal{D}_{kl} \varphi_j^{(l)}, \varphi_i^{(k)} \big\rangle \tag{24}$$

or, in a matrix form

$$\underbrace{\begin{bmatrix} \mathsf{J}_1 + \mathsf{D}_{11} & \mathsf{D}_{12} & \mathsf{D}_{13} & \dots & \mathsf{D}_{1,N} \\ \mathsf{D}_{21} & \mathsf{J}_2 + \mathsf{D}_{22} & \mathsf{D}_{23} & \dots & \mathsf{D}_{2,N} \\ \mathsf{D}_{31} & \mathsf{D}_{32} & \mathsf{J}_3 + \mathsf{D}_{33} & \dots & \mathsf{D}_{3,N} \\ \vdots & \vdots & \vdots & \ddots & \vdots \\ \mathsf{D}_{N,1} & \mathsf{D}_{N,2} & \mathsf{D}_{N,3} & \dots & \mathsf{J}_N + \mathsf{D}_{N,N} \end{bmatrix}}_{\mathsf{A}} \begin{bmatrix} \mathbf{x}_1 \\ \mathbf{x}_2 \\ \mathbf{x}_3 \\ \vdots \\ \mathbf{x}_N \end{bmatrix} = \begin{bmatrix} \mathbf{b}_1 \\ \mathbf{b}_2 \\ \mathbf{b}_3 \\ \dots \\ \mathbf{b}_N \end{bmatrix} \tag{25}$$

where

$$\begin{aligned} \big(\mathsf{J}_k\big)_{ij} &= \frac{\sigma_k + \sigma_{k+1}}{2} \big\langle \varphi_i^{(k)}, \varphi_j^{(l)} \big\rangle \\ \big(\mathsf{D}_{kl}\big)_{ij} &= -(\sigma_{l+1} - \sigma_l) \big\langle \mathcal{D}_{kl} \varphi_j^{(l)}, \varphi_i^{(k)} \big\rangle \\ \big(\mathbf{b}_k\big)_i &= \Big\langle \sum_{l=1}^{N} v_{\Omega_l}, \varphi_i^{(l)} \Big\rangle, \qquad \big(\mathbf{x}_k\big)_i = x_i^{(k)} \end{aligned}$$

[2] Their sum is equal to 1 everywhere.

As in the single-layer case, and thanks to the duality between $\mathcal{D}$ and $\mathcal{D}^*$, the inner integrals needed to calculate elements of matrices D_{lk} have an analytical solution for both P0 and P1 basis functions [19, 28], while the outer integrals are calculated numerically [8]. The matrix is again full, non-symmetric, and needs to be deflated, this time because the potential V is only defined up to a constant (see Appendix J). Imposing the condition $\mathscr{H}$ is impractical, we therefore impose instead either that the overall mean of the potential be zero, $\sum_{k=1}^{N}\sum_i x_i^{(k)} = 0$, or that the mean of the potential on just the external layer be zero, $\sum_i x_i^{(N)} = 0$. In the latter case we propose to modify (deflate) only the bottom-right block of A, namely $\mathsf{J}_{N-1} + \mathsf{D}_{N-1,N-1}$. The basis functions are assumed to satisfy the partition of unity property.

The continuous V is directly accessible from the discretization equation $V(\mathbf{r}) = \sum_i x_i^{(k)}\varphi_i^{(k)}$ for $\mathbf{r} \in S_k$.

4.8 Symmetric approach

The specificity of the discretization of the symmetric case is that both V and its derivative p are simultaneously involved as unknowns. The approximation errors for the two quantities should be asymptotically equivalent, so that the overall error is not dominated by either one. For this reason, we choose to approximate V using P1 basis functions as $V_{S_k}(\mathbf{r}) = \sum_i x_i^{(k)}\phi_i^{(k)}(\mathbf{r})$, while p is represented in the space P0, $p_{S_k}(\mathbf{r}) = \sum_i y_i^{(k)}\psi_i^{(k)}(\mathbf{r})$. Similar concerns guide our choice of test functions. We notice that the operator $\mathcal{S}$ behaves as a smoother: it increases the regularity of its argument [7] by one. The operators $\mathcal{D}$, $\mathcal{D}^*$ do not change it, while $\mathcal{N}$ has a derivative character: it decreases the regularity by one. The regularity is closely tied to an approximation order [33]. To balance the errors, all the scalar products should have the same approximation order. To ensure this, we multiply the equation (18) for the potential (a P1 function) by test functions ψ_i from P0

$$\begin{aligned}
\big\langle \sigma_{k+1}^{-1} v_{\Omega_{k+1}} - \sigma_k^{-1} v_{\Omega_k}, \psi_i^{(k)} \big\rangle = \\
\sum_j x_j^{(k-1)} \big\langle \mathcal{D}_{k,k-1}\phi_j^{(k-1)}, \psi_i^{(k)} \big\rangle - 2\sum_j x_j^{(k)} \big\langle \mathcal{D}_{kk}\phi_j^{(k)}, \psi_i^{(k)} \big\rangle + \\
+ \sum_j x_j^{(k+1)} \big\langle \mathcal{D}_{k,k+1}\phi_j^{(k+1)}, \psi_i^{(k)} \big\rangle - \sigma_k^{-1} \sum_j y_j^{(k-1)} \big\langle \mathcal{S}_{k,k-1}\psi_j^{(k-1)}, \psi_i^{(k)} \big\rangle + \\
+ (\sigma_k^{-1} + \sigma_{k+1}^{-1}) \sum_j y_j^{(k)} \big\langle \mathcal{S}_{kk}\psi_j^{(k)}, \psi_j^{(k)} \big\rangle - \sigma_{k+1}^{-1} \sum_j y_j^{(k+1)} \big\langle \mathcal{S}_{k,k+1}\psi_j^{(k+1)}, \psi_j^{(k)} \big\rangle,
\end{aligned}$$

and the equation (19) for the flow (a P0 function) by test functions ϕ_i from P1

$$\begin{aligned}\left\langle \partial_{\mathbf{n}} v_{\Omega_{k+1}} - \partial_{\mathbf{n}} v_{\Omega_k}, \phi_i^{(k)} \right\rangle = \\ \sigma_k \sum_j x_j^{(k-1)} \left\langle \mathcal{N}_{k,k-1} \phi_j^{(k-1)}, \phi_i^{(k)} \right\rangle - (\sigma_k + \sigma_{k+1}) \sum_j x_j^{(k)} \left\langle \mathcal{N}_{kk} \phi_j^{(k)}, \phi_i^{(k)} \right\rangle + \\ + \sigma_{k+1} \sum_j x_j^{(k+1)} \left\langle \mathcal{N}_{k,k+1} \phi_j^{(k+1)}, \psi_i^{(k)} \right\rangle - \sum_j y_j^{(k-1)} \left\langle \mathcal{D}^*_{k,k-1} \psi_j^{(k-1)}, \phi_i^{(k)} \right\rangle + \\ + 2 \sum_j y_j^{(k)} \left\langle \mathcal{D}^*_{kk} \psi_j^{(k)}, \phi_j^{(k)} \right\rangle - \sum_j y_j^{(k+1)} \left\langle \mathcal{D}^*_{k,k+1} \psi_j^{(k+1)}, \phi_j^{(k)} \right\rangle,\end{aligned}$$

both to hold on all interfaces $k = 1, \ldots, N$. This set of equations can be expressed more concisely in the matrix form

$$\underbrace{\begin{bmatrix} (\sigma_1+\sigma_2)\mathsf{N}_{11} & -2\mathsf{D}^*_{11} & -\sigma_2\mathsf{N}_{12} & \mathsf{D}^*_{12} & & & \\ -2\mathsf{D}_{11} & (\sigma_1^{-1}+\sigma_2^{-1})\mathsf{S}_{11} & \mathsf{D}_{12} & -\sigma_2^{-1}\mathsf{S}_{12} & & & \\ -\sigma_2\mathsf{N}_{21} & \mathsf{D}^*_{21} & (\sigma_2+\sigma_3)\mathsf{N}_{22} & -2\mathsf{D}^*_{22} & -\sigma_3\mathsf{N}_{23} & \mathsf{D}^*_{23} & \\ \mathsf{D}_{21} & -\sigma_2^{-1}\mathsf{S}_{21} & -2\mathsf{D}_{22} & (\sigma_2^{-1}+\sigma_3^{-1})\mathsf{S}_{22} & \mathsf{D}_{23} & -\sigma_3^{-1}\mathsf{S}_{23} & \\ & & -\sigma_3\mathsf{N}_{32} & \mathsf{D}^*_{32} & (\sigma_3+\sigma_4)\mathsf{N}_{33} & -2\mathsf{D}^*_{33} & \cdots \\ & & \mathsf{D}_{32} & -\sigma_3^{-1}\mathsf{S}_{32} & -2\mathsf{D}_{33} & (\sigma_3^{-1}+\sigma_4^{-1})\mathsf{S}_{33} & \cdots \\ & & & & \vdots & \vdots & \ddots \end{bmatrix}}_{\mathsf{A}} \underbrace{\begin{bmatrix} \mathbf{x}_1 \\ \mathbf{y}_1 \\ \mathbf{x}_2 \\ \mathbf{y}_2 \\ \mathbf{x}_3 \\ \mathbf{y}_3 \\ \vdots \end{bmatrix}}_{\mathbf{w}} = \underbrace{\begin{bmatrix} \mathbf{b}_1 \\ \mathbf{c}_1 \\ \mathbf{b}_2 \\ \mathbf{c}_2 \\ \mathbf{b}_3 \\ \mathbf{c}_3 \\ \vdots \end{bmatrix}}_{\mathbf{z}} \tag{26}$$

with

$$\begin{aligned} \left(\mathsf{N}_{kl}\right)_{ij} &= \left\langle \mathcal{N}_{kl} \phi_j^{(l)}, \phi_i^{(k)} \right\rangle & \left(\mathsf{S}_{kl}\right)_{ij} &= \left\langle \mathcal{S}_{kl} \psi_j^{(l)}, \psi_i^{(k)} \right\rangle \\ \left(\mathsf{D}_{kl}\right)_{ij} &= \left(\mathsf{D}^*_{lk}\right)_{ji} = \left\langle \mathcal{D}_{kl} \phi_j^{(l)}, \psi_i^{(k)} \right\rangle & & \\ \left(\mathbf{b}_k\right)_i &= \left\langle \sigma_{k+1}^{-1} v_{\Omega_{k+1}} - \sigma_k^{-1} v_{\Omega_k}, \psi_i^{(k)} \right\rangle & \left(\mathbf{c}_k\right)_i &= \left\langle \partial_{\mathbf{n}} v_k - \partial_{\mathbf{n}} v_{k+1}, \phi_i^{(k)} \right\rangle \\ \left(\mathbf{x}_k\right)_i &= x_i^{(k)} & \left(\mathbf{y}_k\right)_i &= y_i^{(k)} \end{aligned}$$

The matrix A should be truncated[3] as in (20), to account for the zero conductivity $\sigma_{N+1} = 0$.

Note that the matrix is larger than in the single or double-layer cases. However, it is is symmetric and block-diagonal, which means that the actual number of elements to be stored is comparable or even reduced, depending on the number of interfaces. Deflation is needed to avoid the indetermination of V. To impose a zero mean of the potential on the outermost surface, only the bottom-right block with $\mathsf{N}_{N,N}$ is modified to $\mathsf{N}_{N,N} + \omega \mathbf{1}^T \mathbf{1}$, using the heuristics $\omega = \left(\mathsf{N}_{N,N}\right)_{11} / M_N$, as in Section 4.6.

4.9 Acceleration

As the number of mesh elements M grows, the matrix assembly time $O(M^2)$ becomes dominated by the time needed to solve the resulting linear system $O(M^3)$, e.g. by LU

[3] Bottom-right corner of A is not shown here for space reasons.

Table 1: The different methods implemented and their associated labels.

Label	Formulation	φ	ψ
1a	Single Layer	P0	Dirac
1b		P0	P0
1c		P1	P1
2a	Double Layer	P0	Dirac
2b		P0	P0
2c		P1	P1
3	Symmetric	P0	P1

decomposition. Iterative solvers [8, 9, 34] can be used instead, reducing the computational time and only accessing the matrix by matrix-vector multiplications Az. This brings other optimization opportunities such as calculating these products approximately using a fast multipole method (FMM) [11], precorrected-FFT [14, 35] or SVD-based methods. Multiresolution techniques permit to reduce the number of expensive iterations on the finest level by solving first a reduced size problem and using its solution as the starting guess. Multigrid algorithms combine iterations on fine and coarse levels for even faster convergence.

Parallelizing the assembly phase is straightforward as the matrix elements can be calculated independently. Parallel techniques also exist for non-iterative algorithms (SCALAPACK library).

5 Experiments

We have implemented the single-layer, double-layer, and symmetric approaches described in this article. The single and double-layer approaches exist in three discretization variants: with the collocation method ($\tilde{\varphi}_j = \delta_{\mathbf{x}_j}$) using the P0 basis functions φ, and with the Galerkin method ($\tilde{\varphi}_j = \varphi_j$) using both P0 and P1 bases. The symmetric method is discretized using P1 basis functions for V and P0 basis functions for p. Table 1 summarizes the different discretization choices, and indicates the labels by which they are referenced in the text and figures.

5.1 Speed

The speed depends strongly on the optimization and acceleration techniques applied and on the precise task. For example, one may consider that the matrix, once assembled, can be used to solve many problems involving the same geometry. In our experiments, the time needed for the direct assembly of the matrix was of the order of 10 s for our smallest head mesh of 3×42 vertices, and up to about 10 min to assemble the matrices of about 5800×5800 elements, corresponding to the meshes of 3×642 vertices, using a parallel code on a cluster of

workstations. The time needed to solve the linear system of equations varied between 10 ms and 2 min for the same cases. Generally, the assembly time grows quadratically with the number of degrees of freedom, and the solution time as a cube. Collocation methods can be 10 or more times faster than the Galerkin method, depending on the numerical integration method used and the number of integration points needed to get the required accuracy. The single-layer method is about twice as costly as the corresponding double-layer method, as two matrices need to be assembled, the matrix A in (22) in order to solve for the single-layer density, and an additional matrix in order to integrate the potential from equation (23).

5.2 Test cases

Our tests were performed on triangulated spherical surfaces. The choice of a spherical geometry has the advantage that an analytical solution is available [20, 36, 37], thus making it possible to evaluate the accuracy of the different methods. The spherical surfaces were triangulated with progressively finer meshes of 42, 162, 642 and 2562 vertices. We performed two types of experiments. First, using a single surface of radius 1.0, delimiting an inside volume of conductivity 1.0 and an outside volume of zero conductivity. Second, we used three concentric spheres[4] with radii 0.87, 0.92, and 1.0, delimiting volumes with conductivities 1.0, 0.0125, 1.0 and 0.0, from inside towards outside. The sources were unitary current dipoles oriented as $[1\ 0\ 1]/\sqrt{2}$ and placed at distances $r = 0.425, 0.68, 0.765, 0.8075,$ and 0.8415 from the center on the x axis.

We chose to evaluate the analytical solution at the triangle centers for the P0 methods and at vertex points for the others. (This admittedly disadvantages Galerkin methods but it is close to actual use.) We then calculated the relative ℓ_2 error as $\varepsilon = \|\mathbf{v}_{\text{anal}} - \mathbf{v}_{\text{num}}\|_{\ell_2} / \|\mathbf{v}_{\text{anal}}\|_{\ell_2}$, making sure that both $\mathbf{v}_{\text{anal}}$ and $\mathbf{v}_{\text{num}}$ have zero means prior to comparison. Note that some authors linearly scale $\mathbf{v}_{\text{num}}$ to obtain the best fit [10]. This obviously reduces significantly the reported error but is difficult to justify in the context of evaluating the accuracy of a method.

5.3 Error versus dipole position

The first set of experiments (Fig. 5) shows how the accuracy decreases when the current dipole source approaches the surface of discontinuity. We observe that the symmetric approach is much less affected than the other methods in the three-sphere case.

5.4 Error versus mesh density

For a fixed source position ($r = 0.765$), the error decreases as the mesh is refined (Fig. 6). In the three-sphere case we observe that while both collocation variants produce the largest errors (results are completely unreliable), Galerkin methods based on P0 approximations are better, and the best results are provided by the P1 methods, namely by the symmetric

[4] The three-sphere case could not be tested with the finest mesh of 2562 vertices for lack of memory.

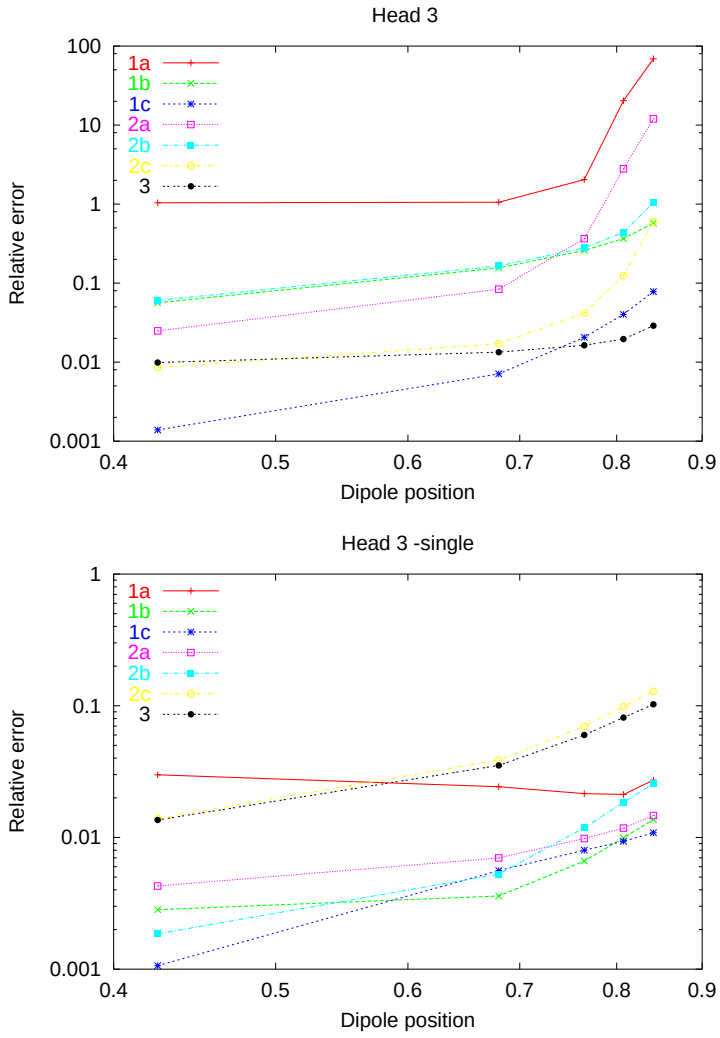

Figure 5: The relative error ε versus the dipole position r for meshes with 642 vertices per sphere. Top: The three-sphere case. Bottom: the one-sphere case. The label 1 (resp. 2) refers to single-layer (resp. double-layer) potential, and the label 3 refers to the symmetric formulation, as explained in Table 1.

formulation. Moreover, the slope of the decrease of the error with mesh size is steeper for P1 methods case, a benefit of their higher approximation order.

5.5 Error versus conductivity

The accuracy of all implemented methods depends on the ratio of conductivities between the second layer (representing the skull) and the neighboring volumes (representing brain and scalp). To display this behavior, we have created additional head models with conductivities of the three volumes $1.0, \sigma, 1.0$, with σ ranging between $1/2$ and $1/1000$. The one-sphere results presented above correspond to a conductivity ratio σ equal to 1. Figure 7 shows that when the conductivity ratio σ becomes small, the precision of the single and double-layer methods drops. The symmetric method displays a clear advantage over the others since, on the contrary, its accuracy increases as $\sigma \to 0$. This is a valuable result in the context of human head modelling where $\sigma \approx 0.01$.

5.6 Discussion

Meaningful comparison of the various techniques is difficult. First, one must bear in mind that they use different number of degrees of freedom to perform the calculations, which moreover is not necessarily identical to the number of degrees of freedom needed to express the solution. More specifically, for a (closed) mesh with N vertices, P1 methods involve N unknowns, P0 based methods use about $2N$ of them, while the symmetric method with P0/P1 discretization uses about $3N$ unknowns, but only N degrees of freedom to express the solution V.

The choice of mesh generation (inscribed over circumscribed, regularity and pole treatment) influences the results. The choice of a spherical geometry itself favors some methods over others. This is why we avoid excessive assumptions about the smoothness of the surface.

The specificity of the single-layer method of representing the solution as an exact term plus a correction makes its performances decrease less drastically than the others. The symmetric method is disadvantaged in the single sphere case, where only the $\mathcal{N}$ operator is used. Finally, the choice of the error measure and the choice of the norm itself (ℓ_2 over ℓ_∞) may favor certain methods over others.

A number of other experiments were performed, only the most relevant are shown here due to space restrictions.

6 Conclusions

We have shown that the classical integral formulation that has been used during the last thirty years in EEG and MEG calculations by the BEM is not unique. We have presented an alternative approach, appealing by its symmetry and its superior accuracy in many cases, and yielding computational savings. The precise theoretical analysis of the accuracy

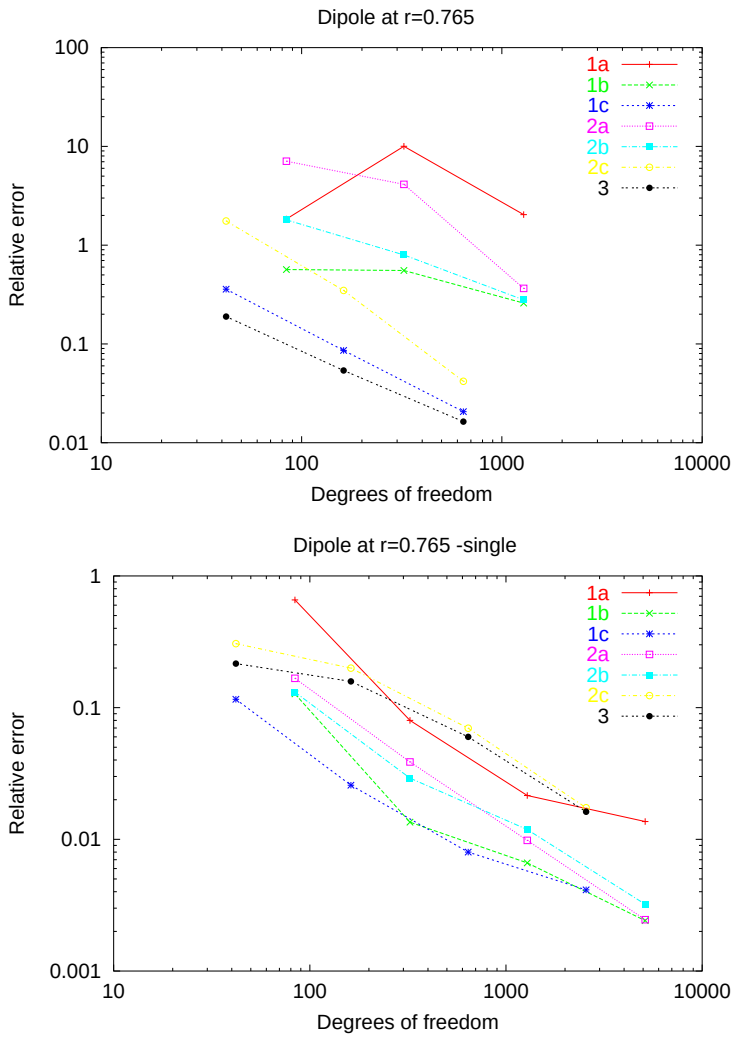

Figure 6: The relative error versus the number of the degrees of freedom of the solution for the dipole source at $r = 0.765$. The three-sphere case is shown on the top, the one-sphere case on the bottom. Both P0 collocation methods in the three-sphere case are outside their area of applicability and do not provide meaningful results. Refer to Table 1 for the meaning of the labels.

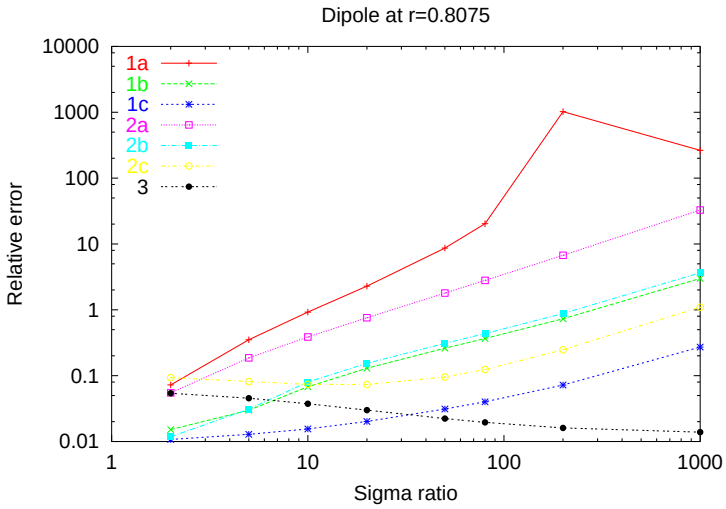

Figure 7: The relative error versus the ratio of conductivities between neighboring layers, for dipole at $r = 0.8075$ and mesh of 642 vertices. Refer to Table 1 for the meaning of the labels.

performance of the different methods is difficult because of the number of factors involved and remains to be done, although some partial results are already present in [7, 25, 38].

The main benefit from using the proposed approach is that the error now increases much less dramatically when the current sources approach the surface of conductivity discontinuity. This implies that we will be able to reduce the number of elements in the mesh for a usable model of the human cortex with a realistic geometry [39], which brings the project of accurate electromagnetic simulation of the human brain much closer to the limits of available technology. Nevertheless, advanced acceleration techniques have to be used both at the algorithm and implementation levels before it becomes viable.

Future work includes better understanding of the accuracy improvements and consequential further development of the method.

APPENDIX: REPRESENTATION THEOREMS

We recall basic identities between surface and volume integrals involving vector fields, leading to the Representation Theorem 1. Note that in this appendix we use an explicit integral notation for didactic purposes, while in the body of the article we have privileged the conciseness of the operator notation (5).

A Green function

Consider a simplified version of Problem (1): the Laplace problem $\Delta u = f$. It is well-known that the so-called Green function (4) is its fundamental solution, i.e. $-\Delta G = \delta_0$ in $\mathbb{R}^3$ in the distributional sense, where δ_0 is the Dirac mass at the origin. By translation invariance, we have

$$-\Delta_{\mathbf{r}} G(\mathbf{r}-\mathbf{r}') = \delta_0(\mathbf{r}-\mathbf{r}') = \delta_{\mathbf{r}'}, \tag{27}$$

where the notation $\Delta_{\mathbf{r}}$ signifies that partial derivatives are taken with respect to the variable $\mathbf{r}$, and $\delta_{\mathbf{r}'}$ is a Dirac mass centered at $\mathbf{r}'$.

There are many fundamental solutions to the Laplace problem, but the Green function (4) is the only one with radial symmetry (a function of the radius $r = \|\mathbf{r}\|$) and vanishing at infinity ($r \to \infty$).

B Green identities

Given a bounded and compact open set $\Omega \subseteq \mathbb{R}^3$ with a regular boundary $\partial\Omega$ which may not be connected, the divergence theorem $\int_\Omega \nabla \cdot \mathbf{g}(\mathbf{r})\,\mathrm{d}\mathbf{r} = \int_{\partial\Omega} \mathbf{g}(\mathbf{r}) \cdot \mathrm{d}\mathbf{s}(\mathbf{r})$ relates the integral over a volume Ω with a surface integral over its boundary $\partial\Omega$. For scalar distributions u, v, substituting $\mathbf{g} = u\,\nabla v$ yields the first Green identity $\int_{\partial\Omega} u\,\nabla v \cdot \mathrm{d}\mathbf{s}(\mathbf{r}) = \int_\Omega \nabla u \cdot \nabla v + u\,\Delta v\ \mathrm{d}\mathbf{r}$. Exchanging u, v and subtracting the resulting equations gives the second[5] Green identity [40]

$$\int_\Omega u\Delta v - v\Delta u\,\mathrm{d}\mathbf{r} = \int_{\partial\Omega} \big(u\,\nabla v - v\nabla u\big) \cdot \mathrm{d}\mathbf{s}(\mathbf{r}) = \int_{\partial\Omega} u\partial_{\mathbf{n}} v - v\partial_{\mathbf{n}} u\,\mathrm{d}s(\mathbf{r})\ ,$$

where $\mathbf{n}$ is normal to $\partial\Omega$, pointing outward (from Ω to its complement $\Omega^c \equiv \mathbb{R}^3 \backslash \overline{\Omega}$). We now choose u to be a harmonic function ($\Delta u = 0$) in Ω, and $v(\mathbf{r}) = -G(\mathbf{r}-\mathbf{r}')$. Using (27) we obtain the third Green identity [6] below, in which $(\partial_{\mathbf{n}} u)^-$ and u^- denote boundary values taken on the inner side of the boundary with respect to the normal $\mathbf{n}$

$$\int_{\partial\Omega} G(\mathbf{r}-\mathbf{r}')(\partial_{\mathbf{n}} u)^-(\mathbf{r}) - u^-(\mathbf{r})\partial_{\mathbf{n}} G(\mathbf{r}-\mathbf{r}')\,\mathrm{d}s(\mathbf{r}) = \begin{cases} u(\mathbf{r}') & \text{if } \mathbf{r}' \in \Omega \\ u^-(\mathbf{r}')/2 & \text{if } \mathbf{r}' \in \partial\Omega \\ 0 & \text{otherwise .} \end{cases} \tag{28}$$

[5] Sometimes called the third. The numbering of Green identities varies among authors.

This important result shows that a harmonic function u inside a volume Ω is completely determined by the internal boundary values of itself and of its normal derivative. To make the notation more compact, we define

$$\mathscr{P}^{\pm}_{S,\mathbf{n}}(u) = \int_S G(\mathbf{r}-\mathbf{r}')\,(\partial_{\mathbf{n}}u)^{\pm} - u^{\pm}(\mathbf{r})\partial_{\mathbf{n}}G(\mathbf{r}-\mathbf{r}')\,\mathrm{d}s(\mathbf{r})$$

and

$$\chi_\Omega\, u(\mathbf{r}) = \begin{cases} u(\mathbf{r}) & \text{if } \mathbf{r}\in\Omega \\ \lim\limits_{\substack{\mathbf{r}'\to\mathbf{r}\\ \mathbf{r}'\in\Omega}} u(\mathbf{r}')/2 & \text{if } \mathbf{r}\in\partial\Omega \\ 0 & \text{if } \mathbf{r}\in\Omega^c\ . \end{cases}$$

Then (28) can be written as

$$\mathscr{P}^{-}_{\partial\Omega,\mathbf{n}}(u) = \chi_\Omega\, u \tag{29}$$

Note that if $\mathbf{r}\in\partial\Omega$, $\lim\limits_{\substack{\mathbf{r}'\to\mathbf{r}\\ \mathbf{r}'\in\Omega}} u(\mathbf{r}') = u^{-}(\mathbf{r})$ with respect to a normal field $\mathbf{n}$ on $\partial\Omega$ pointing outside Ω. This orientation assumed on the left-hand sides of (28) and (29). Considering a normal vector field $\mathbf{n}' = -\mathbf{n}$ which now points *inside* the domain Ω, then partial derivatives change signs, and the third Green identity (28) becomes

$$-\int_{\partial\Omega} G(\mathbf{r}-\mathbf{r}')(\partial_{\mathbf{n}'}u)^{+}(\mathbf{r}) - u^{+}(\mathbf{r})\partial_{\mathbf{n}'}G(\mathbf{r}-\mathbf{r}')\,\mathrm{d}s(\mathbf{r}) = \begin{cases} u(\mathbf{r}') & \text{if } \mathbf{r}'\in\Omega \\ u^{+}(\mathbf{r}')/2 & \text{if } \mathbf{r}'\in\partial\Omega \\ 0 & \text{otherwise}\ , \end{cases}$$

the $'+'$ superscript indicating that the values of u and its normal derivative must this time be considered on the side *towards* which the normal $\mathbf{n}'$ is pointing. Therefore, for an inward-pointing normal field,

$$-\mathscr{P}^{+}_{\partial\Omega,\mathbf{n}'}(u) = \chi_\Omega\, u\ .$$

Note that χ_Ω is intrinsic to Ω, in the sense that it is independent of any normal orientation on $\partial\Omega$.

C Hollow ball topology

Interestingly, the third Green identity (28) is also valid for a hollow ball such as depicted in Fig. 2 as $\Omega = \Omega_2$ with a boundary consisting of two unconnected parts, S_1 and S_2.

The relation (29) supposes that the normal field $\mathbf{n}$ points outside the domain Ω. This is not the case in Figure 2, where the normal field on S_1 (which we call $\mathbf{n}_1$) points inwards, whereas the normal field on S_2 (which we call $\mathbf{n}_2$) points outwards. Decomposing $\partial\Omega = S_1 \cup S_2$, and using the above considerations on the sign of the normal, one can write

$$\chi_\Omega u = -\mathscr{P}^{+}_{S_1,\mathbf{n}_1}(u) + \mathscr{P}^{-}_{S_2,\mathbf{n}_2}(u)\ . \tag{30}$$

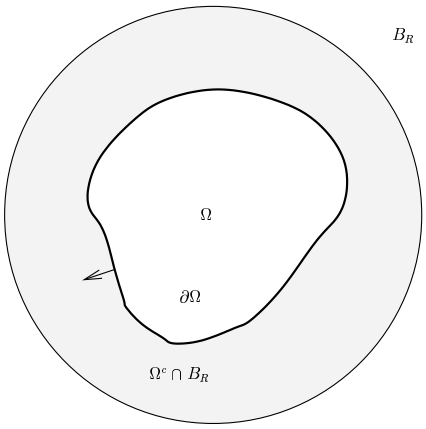

Figure 8: Two-dimensional slice through a volume Ω enclosed within a growing ball B_R, yielding a bounded volume $\Omega^c \cap B_R$ with a hollow ball topology.

D Complement space

Let us now consider a bounded volume Ω with the topology of a sphere. Take its unbounded complement $\Omega^c = \mathbb{R}^3 \backslash \overline{\Omega}$ and try to derive the third Green formula for a function u harmonic in Ω^c and satisfying $\mathscr{H}$. To do this, we consider the (bounded) intersection of Ω^c with a ball B_R of radius R surrounding Ω, as shown in Figure 8. The volume $\Omega^c \cap B_R$ has a hollow ball topology and the Green identities hold. As R tends to infinity, the contribution on ∂B_R gets negligible thanks to both G and u satisfying the condition $\mathscr{H}$. This shows that the third Green identity (28) is also valid in an unbounded space Ω^c, for harmonic functions u satisfying $\mathscr{H}$. It can be written in the compact form:

$$\chi_{\Omega^c}\, u = -\mathscr{P}^{+}_{\partial\Omega,\mathbf{n}}(u)\ . \tag{31}$$

E Representation theorem

Combining the third Green identities for Ω and Ω^c yields the following well-known classical representation theorem, see [6, 7] for a complete proof.

Theorem 2 (Representation Theorem for** u**) *Let $\Omega \subseteq \mathbb{R}^3$ be a bounded open set with a regular boundary $\partial\Omega$. Let $u : (\Omega \cup \Omega^c) \to \mathbb{R}$ be a function harmonic ($\Delta u = 0$) in both Ω and Ω^c, satisfying the $\mathscr{H}$ condition, and let further $p(\mathbf{r}') \stackrel{\text{def}}{=} p_{\mathbf{n}'}(\mathbf{r}') = \partial_{\mathbf{n}'} u(\mathbf{r}')$, where $\mathbf{n}'$ is the outward unit normal of $\partial\Omega$ at point $\mathbf{r}'$. Then for $\mathbf{r} \notin \partial\Omega$ the following representation*

holds:

$$u(\mathbf{r}) = \int_{\partial\Omega} -\partial_{\mathbf{n}'} G(\mathbf{r}-\mathbf{r}')\big[u\big]_{\partial\Omega}(\mathbf{r}') + G(\mathbf{r}-\mathbf{r}')\big[p\big]_{\partial\Omega}(\mathbf{r}')\ \mathrm{d}s(\mathbf{r}') \tag{32a}$$

and for $\mathbf{r} \in \partial\Omega$

$$u^{\pm}(\mathbf{r}) = \mp\frac{[u]_{\partial\Omega}}{2} + \int_{\partial\Omega} -\partial_{\mathbf{n}'} G(\mathbf{r}-\mathbf{r}')\big[u\big]_{\partial\Omega}(\mathbf{r}') + G(\mathbf{r}-\mathbf{r}')\big[p\big]_{\partial\Omega}(\mathbf{r}')\ \mathrm{d}s(\mathbf{r}')\ . \tag{32b}$$

The theorem shows that a function u harmonic in $\Omega \cup \Omega^c$ and satisfying $\mathscr{H}$ is completely determined by the jumps of $[u]$ and $[\partial_{\mathbf{n}} u]$ on the interface $\partial\Omega$. Observe that u from (32a) converges to $(u^+ + u^-)/2$ on $\partial\Omega$, while the value of u jumps when crossing the boundary. This is manifested by the term $\mp\frac{[u]_{\partial\Omega}}{2}$ in (32b).

F Representation theorem for the nested domain topology

Having in view the layered model depicted in Fig. 1, we extend Theorem 2 to a nested domain topology. As we have seen in Section 3.6, it suffices to consider the case of three nested domains as in Fig. 2.

Proposition 1 *Let $\Omega_1, \Omega_2, \Omega_3$ be disjoint open sets such that $\overline{\Omega}_1 \cup \overline{\Omega}_2 \cup \overline{\Omega}_3 = \mathbb{R}^3$, separated by regular boundaries $\partial\Omega_1 \cap \partial\Omega_2 = S_1$, $\partial\Omega_2 \cap \partial\Omega_3 = S_2$, and $\partial\Omega_1 \cap \partial\Omega_3 = \emptyset$. Let $u : \big(\Omega_1 \cup \Omega_2 \cup \Omega_3\big) \to \mathbb{R}$ be harmonic and satisfy $\mathscr{H}$. Then* (32a) *and* (32b) *hold with $\partial\Omega = S_1 \cup S_2$.*

Proof To prove this proposition, we use the third Green identities (29) in Ω_1 and (31) in Ω_3, and the variant (30) in Ω_2. We assume that the normal vector fields $\mathbf{n}_1$ on S_1 and $\mathbf{n}_2$ on S_2 point globally outward (as in Fig. 2). We have

$$\begin{aligned}
\chi_{\Omega_1} u &= \mathscr{P}^-_{S_1,\mathbf{n}_1}(u)\ , \\
\chi_{\Omega_2} u &= -\mathscr{P}^+_{S_1,\mathbf{n}_1}(u) + \mathscr{P}^-_{S_2,\mathbf{n}_2}(u)\ , \\
\chi_{\Omega_3} u &= -\mathscr{P}^+_{S_2,\mathbf{n}_2}(u)\ .
\end{aligned}$$

Summing up the three contributions gives

$$\chi_{\Omega_1} u + \chi_{\Omega_2} u + \chi_{\Omega_3} u = \big(\mathscr{P}^-_{S_1,\mathbf{n}_1}(u) - \mathscr{P}^+_{S_1,\mathbf{n}_1}(u)\big) + \big(\mathscr{P}^-_{S_2,\mathbf{n}_2}(u) - \mathscr{P}^+_{S_2,\mathbf{n}_2}(u)\big)\ .$$

For $\mathbf{r} \in \Omega_1 \cup \Omega_2 \cup \Omega_3$, $\chi_{\Omega_1} u(\mathbf{r}) + \chi_{\Omega_2} u(\mathbf{r}) + \chi_{\Omega_3} u(\mathbf{r}) = u(\mathbf{r})$, and we obtain (32a). For $\mathbf{r} \in S_1 \cup S_2$, $\chi_{\Omega_1} u(\mathbf{r}) + \chi_{\Omega_2} u(\mathbf{r}) + \chi_{\Omega_3} u(\mathbf{r}) = \frac{u^+(\mathbf{r}) + u^-(\mathbf{r})}{2}$. Since $u^+ = -\frac{1}{2}[u]_{\partial\Omega} + \frac{u^+ + u^-}{2}$ and $u^- = \frac{1}{2}[u]_{\partial\Omega} + \frac{u^+ + u^-}{2}$, we obtain (32b).
□

G Single and double-layer potentials

The *single-layer potential* (the second part of (32a)) is given explicitly as

$$u_s(\mathbf{r}) = \int_{\partial\Omega} G(\mathbf{r}-\mathbf{r}')\xi(\mathbf{r}')\,\mathrm{d}s(\mathbf{r}') \tag{33}$$

while the *double-layer potential* (the first part of (32a)) is written as

$$u_d(\mathbf{r}) = \int_{\partial\Omega} \partial_{\mathbf{n}'} G(\mathbf{r}-\mathbf{r}')\mu(\mathbf{r}')\,\mathrm{d}s(\mathbf{r}'). \tag{34}$$

The function ξ corresponds to a charge density distribution on $\partial\Omega$, while μ may be viewed as a dipole density. Both potentials (33), (34) satisfy the Laplace equation $\Delta u = 0$ in $\Omega \cup \Omega^c$ and also satisfy the condition $\mathscr{H}$. Remarkably, with arbitrary functions ξ, μ from $C^0(\partial\Omega)$, both (33) and (34) yield a harmonic function in $C^2(\Omega \cup \Omega^c)$.

The single-layer potential is continuous with respect to $\mathbf{r}$, in particular when crossing the boundary $\partial\Omega$. On the other hand its normal derivative is discontinuous when crossing $\partial\Omega$. As proved in [7], the limit values on both sides are

$$p^{\pm}_{\mathbf{n}}(\mathbf{r}) = \partial_{\mathbf{n}} u^{\pm}(\mathbf{r}) = \mp\frac{\xi(\mathbf{r})}{2} + \int_{\partial\Omega} \partial_{\mathbf{n}} G(\mathbf{r}-\mathbf{r}')\xi(\mathbf{r}')\,\mathrm{d}s(\mathbf{r}') \qquad \text{for } \mathbf{r} \in \partial\Omega \tag{35}$$

The double-layer potential enjoys the opposite properties. It has a discontinuity when crossing $\partial\Omega$ and the corresponding limit values on both sides of $\partial\Omega$ are

$$u^{\pm}(\mathbf{r}) = \pm\frac{\mu(\mathbf{r})}{2} + \int_{\partial\Omega} \partial_{\mathbf{n}'} G(\mathbf{r}-\mathbf{r}')\mu(\mathbf{r}')\,\mathrm{d}s(\mathbf{r}') \qquad \text{for } \mathbf{r} \in \partial\Omega \tag{36}$$

The normal derivative of a double-layer potential is continuous when crossing $\partial\Omega$. Taking the derivative of (34) in the direction $\mathbf{n}$ at $\mathbf{r}$, we write

$$p(\mathbf{r}) = p_{\mathbf{n}}(\mathbf{r}) = \partial_{\mathbf{n}} u(\mathbf{r}) = \int_{\partial\Omega} \partial^2_{\mathbf{n},\mathbf{n}'} G(\mathbf{r}-\mathbf{r}')\mu(\mathbf{r}')\,\mathrm{d}s(\mathbf{r}')\ . \tag{37}$$

A subtle point here is that the kernel $\partial^2_{\mathbf{n},\mathbf{n}'} G(\mathbf{r}-\mathbf{r}')$ is not an integrable function for $\mathbf{r}' \to \mathbf{r}$. We therefore need to treat p as a distribution, defined through scalar products with suitable test functions. This is unlike $[p]$ which is continuous on $\partial\Omega$.

Given these definitions, we can reinterpret (32a) as showing that a function u harmonic in $\Omega \cup \Omega^c$ is represented as the sum of a single-layer potential [6, 7] corresponding to $\xi = [p]$ and a double-layer potential corresponding to $\mu = -[u]$.

H Multiple interface potentials

The single and double potentials can also easily be applied in the case of our layered model from Fig.1. For the single-layer potential, we write:

$$u_s(\mathbf{r}) = \sum_{i=1}^{N} \int_{S_i} G(\mathbf{r}-\mathbf{r}')\xi_{S_i}(\mathbf{r}')\,\mathrm{d}s(\mathbf{r}') \tag{38}$$

where each ξ_{S_i} is defined on the corresponding surface S_i. The properties from the single interface case are trivially satisfied thanks to additivity, namely $[u_s]_i = 0$ and $[\partial_{\mathbf{n}} u_s]_i = \xi_i$. More specifically,

$$p^{\pm}_{\mathbf{n}}(\mathbf{r}) = \partial_{\mathbf{n}} u^{\pm}_s(\mathbf{r}) = \mp\frac{\xi_{S_j}(\mathbf{r})}{2} + \sum_{i=1}^{N} \int_{S_i} \partial_{\mathbf{n}} G(\mathbf{r}-\mathbf{r}')\xi_{S_i}(\mathbf{r}')\,\mathrm{d}s(\mathbf{r}') \qquad \text{for } \mathbf{r} \in S_j\ . \tag{39}$$

Similarly, for the double-layer potential, we have

$$u_d(\mathbf{r}) = \sum_{i=1}^{N-1} \int_{S_i} \partial_{\mathbf{n}'} G(\mathbf{r}-\mathbf{r}')\mu_{S_i}(\mathbf{r}')\,\mathrm{d}s(\mathbf{r}')\ , \tag{40}$$

with $[u_d]_i = -\mu_{S_i}$, $[\partial_{\mathbf{n}} u_d] = 0$ and

$$u^{\pm}_d(\mathbf{r}) = \pm\frac{\mu_{S_j}(\mathbf{r})}{2} + \sum_{i=1}^{N} \int_{S_i} \partial_{\mathbf{n}'} G(\mathbf{r}-\mathbf{r}')\mu_{S_i}(\mathbf{r}')\,\mathrm{d}s(\mathbf{r}') \qquad \text{for } \mathbf{r} \in S_j\ . \tag{41}$$

I Extended representation theorem

The equations concerning p in Sections G are summarized in Theorem 3 below, which extends Theorem 2 to the directional and normal derivatives of u.

Theorem 3 (Representation Theorem for** p**) *Let $\Omega \subseteq \mathbb{R}^3$ be a bounded open set with a regular boundary $\partial\Omega$. Let $u : (\Omega \cup \Omega^c) \to \mathbb{R}$ be a function harmonic ($\Delta u = 0$) in both Ω and Ω^c , satisfying condition $\mathscr{H}$. Let also $\mathbf{n}$ (resp. $\mathbf{n}'$) be the unit normal to $\partial\Omega$ at point $\mathbf{r}$ (resp. $\mathbf{r}'$) and $\mathbf{m}$ an arbitrary unit vector at $\mathbf{r}$. Then for $\mathbf{r} \notin \partial\Omega$ the following representation holds:*

$$p_{\mathbf{m}}(\mathbf{r}) = \int_{\partial\Omega} -\partial^2_{\mathbf{m},\mathbf{n}'} G(\mathbf{r}-\mathbf{r}')\big[u\big]_{\partial\Omega}(\mathbf{r}') + \partial_{\mathbf{m}} G(\mathbf{r}-\mathbf{r}')\big[p\big]_{\partial\Omega}(\mathbf{r}')\,\mathrm{d}s(\mathbf{r}') \tag{42a}$$

and for $\mathbf{r} \in \partial\Omega$

$$p^{\pm}(\mathbf{r}) \stackrel{def}{=} p^{\pm}_{\mathbf{n}}(\mathbf{r}) = \mp\frac{[p]_{\partial\Omega}}{2} + \int_{\partial\Omega} -\partial^2_{\mathbf{n},\mathbf{n}'} G(\mathbf{r}-\mathbf{r}')\big[u\big]_{\partial\Omega}(\mathbf{r}') + \partial_{\mathbf{n}} G(\mathbf{r}-\mathbf{r}')\big[p\big]_{\partial\Omega}(\mathbf{r}')\,\mathrm{d}s(\mathbf{r}') \ . \tag{42b}$$

Analogously to u, the derivative $p = p_{\mathbf{n}}$ given by (42a) for $\mathbf{m} = \mathbf{n}$ converges to $p = (p^+ + p^-)/2$ on $\partial\Omega$ in the distributional sense. Theorem 3 also holds in the case of a nested volume topology, but we do not provide the detailed proof here.

J Uniqueness

The integral representation in terms of $\mu = -[u]$ and $\xi = [p]$ is unique, if u and p are considered as a pair [7]. In other words, there is only one pair of (μ, ξ) generating a given (u^-, p^-), (u^+, p^+), or $([u], [p])$. However, this is no longer true if only p^- is given (interior Neumann problem), as any constant function can be added to u. Physically, this means that the potential is only known up to a constant. To get rid of this indetermination, we can for example choose to impose $\langle u, 1\rangle = 0$; other options are possible [32]. In the same spirit, note that for harmonic u, the Stokes theorem necessarily imposes $\langle p, 1\rangle = 0$ on any closed surface.

K Weak regularity

We shall need to extend Theorems 2,3 also for non-regular surfaces[6], such as for example a triangulated surface which is not regular on the edges and at the vertices. We find that the equations in Theorems 2 and 3 hold, provided that there are not "too many" singular points (their set is of zero measure) and that we only evaluate the integrals in (32b), (42b) at the regular points. If needed, the values/limits on the surface can still be calculated even in the singular points by a more complex expression involving inner and outer spherical angles [10, 41]. We will avoid this complication here by concentrating on the Galerkin method that gives better results and does not require pointwise values.

In a similar vein, we can relax the continuity requirements on $\mu = -[u]$, $\xi = [p]$, in order to approximate them by some $\tilde{\mu}$, $\tilde{\xi}$. Only piecewise continuity is necessary for the convergence of the integrals in Theorems 2,3 (again with a set of discontinuity points of zero measure) if we do not evaluate (32b),(42b) at the points of discontinuity.

[6] A surface is regular if it can be locally approximated by a linear function everywhere.

References

[1] J. W. Phillips, R. M. Leahy, J. C. Mosher, and B. Timsari, "Imaging neural activity using MEG and EEG," *IEEE Eng. Med. Biol.*, pp. 34–41, May 1997.

[2] Jukka Sarvas, "Basic mathematical and electromagnetic concepts of the biomagnetic inverse problem," *Phys. Med. Biol.*, vol. 32, no. 1, pp. 11–22, 1987.

[3] Matti Hämäläinen, Riitta Hari, Risto J. IImoniemi, Jukka Knuutila, and Olli V. Lounasmaa, "Magnetoencephalography— theory, instrumentation, and applications to noninvasive studies of the working human brain," *Reviews of Modern Physics*, vol. 65, no. 2, pp. 413–497, Apr. 1993.

[4] D. B Geselowitz, "On the magnetic field generated outside an inhomogeneous volume conductor by internal volume currents," *IEEE Trans. Magn.*, vol. 6, pp. 346–347, 1970.

[5] O. Faugeras, F. Clément, R. Deriche, R. Keriven, T. Papadopoulo, J. Roberts, T. Viéville, F. Devernay, J. Gomes, G. Hermosillo, P. Kornprobst, and D. Lingrand, "The inverse EEG and MEG problems: The adjoint space approach I: The continuous case," Tech. Rep. 3673, INRIA, May 1999.

[6] Marc Bonnet, *Equations intégrales et éléments de frontière*, CNRS Editions, Eyrolles, 1995.

[7] Jean-Claude Nédélec, *Acoustic and Electromagnetic Equations*, Springer Verlag, 2001.

[8] J. Rahola and S. Tissari, "Iterative solution of dense linear systems arising from the electrostatic integral equation," *Phys. Med. Biol.*, , no. 47, pp. 961–975, 2002.

[9] Jussi Rahola and Satu Tissari, "Iterative solution of dense linear systems arising from boundary element formulations of the biomagnetic inverse problem," Tech. Rep. TR/PA/98/40, CERFACS, 1998, Toulouse, France.

[10] A. Steward Ferguson and Gerhard Stroink, "Factors affecting the accuracy of the boundary element method in the forward problem — I: Calculating surface potentials," *IEEE Trans. Biomed. Eng.*, vol. 44, no. 11, pp. 1139–1155, Nov. 1997.

[11] Maureen Clerc, Renaud Keriven, Olivier Faugeras, Jan Kybic, and Theo Papadopoulo, "The fast multipole method for the direct E/MEG problem," in *Proceedings of ISBI*, Washington, D.C., July 2002, IEEE, NIH.

[12] Satu Tissari and Jussi Rahola, "Error analysis of a new Galerkin method to solve the forward problem in MEG and EEG using the boundary element method," Tech. Rep. TR/PA/98/39, CERFACS, 1998, Toulouse, France.

[13] M. S. Hämäläinen and J. Sarvas, "Realistic conductivity geometry model of the human head for interpretation of neuromagnetic data," *IEEE Trans. Biomed. Eng.*, vol. 36, no. 2, pp. 165–171, Feb. 1989.

[14] S. Tissari and J. Rahola, "A precorrected-FFT method to accelerate the solution of the forward problem in MEG," in *Proceedings of BIOMAG*, 2002.

[15] Zhi Zhang and Don L. Jewett, "Insidious errors in dipole localization parameters at a single time-point due to model misspecification of number of shells," *Electroencephalography and clinical Neurophysiology*, , no. 88, pp. 1–11, 1993.

[16] R.M. Leahy, J.C. Mosher, M.E. Spencer, M.X. Huang, and J.D. Lewine, "A study of dipole localization accuracy for MEG and EEG using a human skull phantom," Los Alamos Technical Report LA-UR-98-1442, Los Alamos National Laboratory, Mar. 1998, Revision of LA-UR-97-4804.

[17] D. B. Geselowitz, "On bioelectric potentials in an homogeneous volume conductor," *Biophysics Journal*, vol. 7, pp. 1–11, 1967.

[18] F. Babiloni, C. Del Gratta, F. Carducci, C. Babiloni, G. M. Roberti, V. Pizzella, P. M. Rossini, G. L. Romani, and A. Urbano, "Combined high resolution EEG and MEG data for linear inverse estimate of human event-related cortical activity," in *Proceedings of the 20th annual int. conf. of the IEEE Eng. Med. Biol. Society*, 1998, number 4, pp. 2151–2154.

[19] J. C. de Munck, "A linear discretization of the volume conductor boundary integral equation using analytically integrated elements," *IEEE Trans. Biomed. Eng.*, vol. 39, no. 9, pp. 986–990, Sept. 1992.

[20] John C. Mosher, Richard B. Leahy, and Paul S. Lewis, "EEG and MEG: Forward solutions for inverse methods," *IEEE Transactions on Biomedical Engineering*, vol. 46, no. 3, pp. 245–259, Mar. 1999.

[21] John C. Mosher, Richard M. Leahy, and Paul S. Lewis, "Matrix kernels for the forward problem in EEG and MEG," Tech. Rep. LA-UR-97-3812, Los Alamos, 1997.

[22] Nevzat G. Gencer and I. Oğuz Tanzer, "Forward problem solution of electromagnetic source imaging using a new BEM formulation with high-order elements," *Phys. Med. Biol.*, vol. 44, no. 9, pp. 2275–2287, 1999.

[23] L. J. Gray and Glaucio H. Paulino, "Symmetric Galerkin boundary integral formulation for interface and multi-zone problems," *Internat. J. Numer. Methods Eng.*, vol. 40, no. 16, pp. 3085–3103, 1997.

[24] J. B. Layton, S. Ganguly, C. Balakrishna, and J. H. Kane, "A symmetric Galerkin multi-zone boundary element formulation," *Internat. J. Numer. Methods Eng.*, vol. 40, no. 16, pp. 2913–2931, 1997.

[25] Snorre H. Christiansen, *Résolution des équations intégrales pour la diffraction d'ondes acoustiques et électromagnétiques*, Ph.D. thesis, Ecole Polytechnique, 2002.

[26] Jyrki Lötjönen, *Construction of Boundary Element Models in Bioelectromagnetism*, Ph.D. thesis, Helsinki University of Technology, Espoo, Finland, 2000.

[27] D. Van 't Ent, J. C. De Munck, and A. L. Kaas, "A fast method to derive realistic BEM models for E/MEG source reconstruction," *IEEE Trans. Biomed. Eng.*, vol. 48, no. 12, Dec. 2001.

[28] D. R. Wilton, S. M. Rao, A. W. Glisson, D. H. Schaubert, O. M. Al-Bundak, and C. M. Butler, "Potential integrals for uniform and linear source distributions on polygonal and polyhedral domains," *IEEE Trans. Antenn. Propag.*, vol. 32, no. 3, pp. 276–281, Mar. 1984.

[29] A. S. Ferguson, X. Zhang, and G. Stroink, "A complete linear discretization for calculating the magnetic field using the boundary element method," *IEEE Trans. Biomed. Eng.*, vol. 41, no. 5, pp. 455–459, May 1994.

[30] J. N. Lyness and D. Jespersen, "Moderate degree symmetric quadrature rules for the triangle," *J. Inst. Maths Applics*, vol. 15, pp. 19–32, 1975.

[31] T. F. Chan, "Deflated decomposition solution of nearly singular systems," *SIAM J. Numer. Anal.*, vol. 21, pp. 739–754, 1984.

[32] G. Fischer, B. Tilg, R. Modre, F. Hanser, B. Messnarz, and P. Wach, "On modeling the Wilson terminal in the Boundary and Finite Element Method," *IEEE Trans. Biomed. Eng.*, vol. 49, no. 3, pp. 217–224, Mar. 2002.

[33] G. Strang and G. Fix, "A Fourier analysis of the finite element variational method," in *Constructive Aspect of Functional Analysis*, pp. 796–830. Cremonese, Rome, Italy, 1971.

[34] Richard Barret, Michael Berry, Tony F. Chan, James Demmel, June Donato, Jack Dongarra, Victor Eijkhout, Roldan Pozo, Charles Romine, and Henk van der Vonst, *Templates for the Solution of Linear Systems: Building Blocks for Iterative Methods*, SIAM, Philadelphia, 1994, Available from netlib.

[35] J. R. Phillips and J. K. White, "A precorrected-FFT method for electrostatic analysis of complicated 3-D structures," *IEEE Trans. CAD Int. Circ. Syst.*, vol. 16, no. 10, Oct. 1997.

[36] J. C. De Munck, "The potential distribution in a layered anisotropic spheroidal volume conductor," *J. Appl. Phys*, vol. 2, no. 64, pp. 464–470, July 1988.

[37] Zhi Zhang, "A fast method to compute surface potentials generated by dipoles within multilayer anisotropic spheres," *Phys. Med. Biol.*, vol. 40, pp. 335–349, 1995.

[38] U. Schmitt, A. K. Louis, F. Darvas, H. Buchner, and M. Fuchs, "Numerical aspects of spatio-temporal current density reconstruction from EEG/MEG-data," *IEEE Trans. Med. Imag.*, vol. 20, no. 4, pp. 314–324, 2001.

[39] R. Van Uitert and C. Johnson, "Can a spherical model substitute for a realistic head model in forward and inverse MEG simulations?," in *Proceedings of BIOMAG*, 2002.

[40] L.C. Evans, *Partial Differential Equations*, vol. 19 of *Graduate Studies in Mathematics*, Proceedings of the American Mathematical Society, 1998.

[41] J. W. H. Meijs, O. W. Weier, M. J. Peters, and A. van Oosterom, "On the numerical accuracy of the boundary element method," *IEEE Trans. Biomed. Eng.*, vol. 36, pp. 1038–1049, 1989.

Contents

1 Introduction **3**
1.1 Problem definition . . . 3
1.2 Notation . . . 3
1.3 Connected Laplace problems . . . 4
1.4 Boundary Element Method . . . 4
1.5 Inaccuracy of BEM implementations . . . 5
1.6 Proposed new integral formulation . . . 5
1.7 Existing work . . . 5
1.8 Organization of this article . . . 5

2 Representation theorem **6**
2.1 Single and double-layer potentials . . . 8

3 Integral formulations **8**
3.1 Dipole source . . . 8
3.2 Homogeneous solution . . . 9
3.3 Multiple domains . . . 9
3.4 Single-layer approach . . . 10
3.5 Double-layer approach . . . 10
3.6 Symmetric approach . . . 11

4 Discretization and implementation **13**
4.1 Discretization of the boundaries . . . 13
4.2 Discretization of the unknowns . . . 13
4.3 Test functions . . . 15
4.4 Galerkin methods . . . 15
4.5 Single-layer formulation . . . 15
4.6 Deflation . . . 17
4.7 Double-layer formulation . . . 17
4.8 Symmetric approach . . . 18
4.9 Acceleration . . . 19

5 Experiments **20**
5.1 Speed 20
5.2 Test cases 21
5.3 Error versus dipole position 21
5.4 Error versus mesh density 21
5.5 Error versus conductivity 23
5.6 Discussion 23

6 Conclusions **23**

A Green function **26**

B Green identities **26**

C Hollow ball topology **27**

D Complement space **28**

E Representation theorem **28**

F Representation theorem for the nested domain topology **29**

G Single and double-layer potentials **30**

H Multiple interface potentials **31**

I Extended representation theorem **31**

J Uniqueness **32**

K Weak regularity **32**

Unité de recherche INRIA Sophia Antipolis
2004, route des Lucioles - BP 93 - 06902 Sophia Antipolis Cedex (France)

Unité de recherche INRIA Lorraine : LORIA, Technopôle de Nancy-Brabois - Campus scientifique
615, rue du Jardin Botanique - BP 101 - 54602 Villers-lès-Nancy Cedex (France)
Unité de recherche INRIA Rennes : IRISA, Campus universitaire de Beaulieu - 35042 Rennes Cedex (France)
Unité de recherche INRIA Rhône-Alpes : 655, avenue de l'Europe - 38330 Montbonnot-St-Martin (France)
Unité de recherche INRIA Rocquencourt : Domaine de Voluceau - Rocquencourt - BP 105 - 78153 Le Chesnay Cedex (France)

Éditeur
INRIA - Domaine de Voluceau - Rocquencourt, BP 105 - 78153 Le Chesnay Cedex (France)
http://www.inria.fr
ISSN 0249-6399